Wave-packet Dynamics in Unconventional RMT Models

by

James Aisenberg
Class of 2009

A thesis submitted to the
faculty of Wesleyan University
in partial fulfillment of the requirements for the
Degree of Bachelor of Arts
with Departmental Honors in Physics

Abstract

We analyze the wave-packet dynamics scenario produced by Random Matrix Theory models with unconventional band-profile structures. Our motivation is to understand the energy spreading of quantum systems with complex dynamics. Examples of such systems include complex nuclei, atoms and molecules, quantum dots, and Bose-Einstein Condensates in optical traps, which, under the influence of an external perturbation, experience an energy redistribution of the initially prepared state. Such a perturbation could be due to an external electric or magnetic field, a change in the confining geometry, or a residual interaction, among other things. Of special interest in our analysis is the investigation of the time relaxation properties of a prepared state into a sea of other states (the continuum). We find that, for a large family of power spectra characterized by a non-flat profile, the survival probability $P(t)$ might exhibit either exponential-like or power-law decay, depending on non-universal features of the model. Still there is a universal characteristic time t_0 that does not depend on the functional form of the survival probability decay. It is only for a flat power spectrum that we get a robust exponential decay that is insensitive to the nature of the intra-continuum couplings. Our analysis highlights the coexistence of perturbative and non-perturbative features in the local density of states.

Acknowledgments

I would like to thank my family, Mom, Dad, Jon and Katie, for your love and support. I also sincerely thank my advisor, Tsampikos Kottos, whose dedication is unrivaled.

Very productive discussions with Doron Cohen and Itamar Sela are greatly acknowledged. I also acknowledge the hospitality of the BGU of the Negev, where part of this work was performed, and the US-Israel Binational Science Foundation (BSF) for support.

Contents

1 Introduction

The central insight of Random Matrix Theory (RMT) modeling is that there is a broad category of systems called complex quantum systems that have statistical properties that are indistinguishable from the statistical properties of ensembles of random matrices of large dimension. The results of RMT are universal, meaning they are largely independent of the characteristics of any particular system. This insight was introduced by Wigner while studying the statistical properties of the spectra of complex nuclei [1]. The theory was extended significantly by Dyson, Mehta, Porter and others, who showed that many of the relevant statistical properties of RMT ensembles can be computed analytically [2]. In recent years, RMT has become a major theoretical tool in the field of quantum chaos [3], and it has found applications in many areas of physics ranging from nuclear, atomic and molecular physics to mesoscopic and mathematical physics (for a review see [4]).

Standard RMT models capture the universal aspects of complex systems [3, 5, 4]. However, in reality, there are also non-universal semi-classical structures that make the use of general RMT inappropriate in particular situations. The study of such structures is a major theme in past works regarding spectral [6] and wave-

function statistics [7, 8]. Ten years ago, Cohen and Kottos initiated the study of various time-dependent scenarios within the framework of RMT modeling, comparing the outcomes with those that have been obtained for real (non-RMT) quantized Hamiltonians [9, 10, 11, 12, 13, 14, 15, 16]. Their main conclusion is that a non-structured band-profile, as assumed in the standard RMT model, is merely an idealization of "generic chaos."

In the present thesis, we bring, for the first time, this theme into a new arena: the theory of wave-packet dynamics in energy space, and we contrast our results with the results of traditional RMT originally due to Wigner. Specifically, we introduce a class of models with structured band-profiles that show distinct deviations from previous studies. The most striking of our results is the identification of a power-law relaxation process, in contrast to the expected and celebrated Fermi Golden Rule (FGR) exponential decay.

The structure of the thesis is as follows:

- In Chapter 2 we will discuss the importance of parametric RMT models to describe physical systems. We will connect a classical quantity (the power spectrum of the fluctuations of the generalized force) with the band-profile of the perturbation matrix. Many physical situations will be discussed that can be studied using this methodology.

- Chapter 3 develops universal results from conventional RMT. The static properties of the frequently encountered ensembles will be established. The objective is to clearly understand the universal aspects of the eigenvalues and eigenfunctions of these ensembles, so the non-universal features of particular

systems can be appreciated.

- Chapter 4 reviews the dynamical properties of conventional RMT. Specifically, we present the wave-packet dynamics scenario for an ensemble of banded random matrices with flat band-profile. To this end, we first analyze a much simpler system, associated with the decay of a bound state into the flat continuum in order to see more clearly how the Fermi Golden Rule decay emerges in such types of problems. We then use these results to understand the time relaxation of the more physical Banded Random Matrix (BRM) model.

- Chapter 5 is based on our recent contribution [17]. We consider the dynamical properties of ensembles of non-flat (structured band-profile) banded random matrices. Following the approach of Chapter 4, we first analyze the dynamics of a simplified system. Surprisingly, we find that the two models follow different relaxation laws. Even though these laws take on different functional forms, they still show limited agreement for a scaling law, indicating the coexistence of perturbative and non-perturbative features in the LDoS.

- Chapter 6 includes some brief concluding remarks that situates the thesis in the context of current research in the field.

Our results (Chapter 5 and [17]) show, for the first time, how non-universal features can lead to a relaxation process that is fundamentally different from the standard Wigner (FGR) decay. As such, they constitute a major step towards un-

derstanding quantum dissipation problems in the presence of semi-classical structures.

2 Parametric Hamiltonians and Physical Setups

The random matrix approach has been extended in several directions. In this chapter we will be concerned with an extension of the approach to deal with physical systems where the Hamiltonian $\mathcal{H}$ depends on some x. In general, x is time dependent, i.e., $x = x(t)$.

The prototypical system described by a parametric Hamiltonian is the piston model, where a gas is contained inside a cavity, and $x(t)$ represents the position of a piston at time t. Our interest is in the case where we have a "one particle gas" (note, however, that for low temperatures the solution of the one particle system can be adapted to describe a gas of many weakly interacting particles). This setup is shown in Figure 2.1 *(left)*. The model assumes that the mass of the piston is large compared to the mass of the particle. This ensures that the collision of the particle with the piston does not affect the motion of the piston. A quantum system that can be described by this model would be an electron cloud of a large molecule. The "piston" in this case is the nucleus of the atom, and the

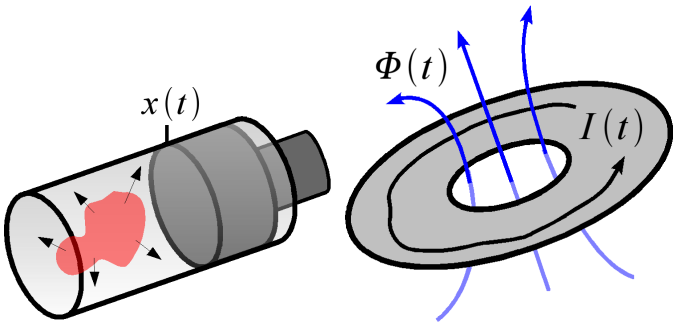

Figure 2.1: *(left)* The piston model, *(right)* The conducting ring. Reproduced from [18] with permission.

cavity is an approximation of the electric potential trapping the electrons near the nucleus. A renewed interest in this model is anticipated in mesoscopic physics, where the shape of a quantum dot can be controlled by gate voltages. In such a case, $v = \dot{x}$ has the interpretation of the piston's velocity. Furthermore, we can argue that there is a friction force proportional to the velocity v, against which the piston is doing mechanical work. This mechanical work is dissipated, and the gas heats up at a rate proportional to v^2.

Another physical system described by parametric Hamiltonians is a dirty conducting ring containing a charged particle. This is depicted in Figure 2.1 *(right)*. In this context, the parameter $\phi(t)$ is the magnetic flux through the hole in the ring. The time derivative of the flux is the electromotive force induced on the particle by Faraday's law ($\epsilon = -\dot{\phi}(t)$). This e.m.f. establishes a current around the ring that is proportional to the e.m.f. itself. The proportionality factor is the conductance G. This is, in fact, "Ohm's Law." The dissipated energy can either be accumulated by the electrons (as kinetic energy), or else it may be transferred

to the lattice vibrations (phonons). In the latter case, we say that the ring is heating. The rate of heating varies like ϵ^2, which is a statement of Joule's law. This is a very convenient model for electrical conduction because it does not involve open geometries.

2.1 Semi-classical Considerations and Random Matrix Theory Models

2.1.1 Classical Considerations

Suppose that $\mathcal{H}(x(t))$ is a classical chaotic Hamiltonian that depends on the parameter $x(t)$. Define $\delta x = x(t) - x(0)$. We assume that δx is classically small, which means that both $\mathcal{H}(x(0))$ and $\mathcal{H}(x(t))$ are generators of the same chaotic classical dynamics. It is then possible to expand $\mathcal{H}$ to first order about $x(0)$:

$$\mathcal{H}(x(t)) = \mathcal{H}(x(0)) + \delta x V \tag{2.1}$$

for some V, which is due to the perturbation. From the analogy of Newtonian mechanics, it is reasonable to define the **generalized force** to be,

$$\mathcal{F}(t) \equiv -\frac{\partial \mathcal{H}}{\partial x} \tag{2.2}$$

with mean value $F = \langle \mathcal{F}(t) \rangle$. The angular brackets denote an averaging that is either micro-canonical over some initial conditions or temporal (due to the

assumed ergodicity). In the case where x is the displacement of the piston (or wall element of a quantum dot), the fluctuating quantity $\mathcal{F}(t)$ has the meaning of a Newtonian force. In the situation where x is the magnetic flux, then $\mathcal{F}(t)$ represents the electric current. A quantity that will be useful later on in the argument is the **autocorrelation function**, $C(\tau)$, of $\mathcal{F}$ which is defined to be,

$$C(\tau) = \langle [\mathcal{F}(t) - F][\mathcal{F}(t+\tau) - F] \rangle \tag{2.3}$$

where again the averaging is either micro-canonical or temporal.

For generic chaotic systems (described by smooth Hamiltonians), the autocorrelation function behaves as $C(\tau) \sim e^{-t/\tau_{\rm cl}}$, i.e., the fluctuations are characterized by a short correlation time $\tau_{\rm cl}$, after which the correlations are negligible. In generic circumstances, $\tau_{\rm cl}$ is essentially the ergodic time, which is related to the Lyapunov exponent, λ by $\tau_{\rm cl} \sim 1/\lambda$. The corresponding energy scale $\omega_c = 1/\tau_{\rm cl}$ is also known in the literature as the "non-universal" energy scale [19], or (in case of diffusive motion) as the Thouless energy [20].

2.1.2 Semi-classical Considerations

One can show that, in the semi-classical limit, there is a strong relationship between the structure of a Hamiltonian of a quantum system in the basis of the unperturbed Hamiltonian and the power spectrum of the perturbation operator.

Let $\mathcal{H} = \mathcal{H}_0 + \delta x V$ be some Hamiltonian. Specifically, we will show that,

$$\left\langle |V_{jk}|^2 \right\rangle_j = \frac{\tilde{C}\left(\omega = \frac{E_j - E_k}{\hbar}\right)}{2\pi g(E_k)} \tag{2.4}$$

where $\tilde{C}(\omega)$ is the power spectrum of V in the classical limit, and g is the density of states. This argument is due to Feingold and Peres [21] (see also Prosen [22]). Let us start our analysis by writing the correlator in the interaction picture, so we will have:

$$\begin{aligned}
\sum_k e^{i(E_j - E_k)\tau/\hbar} |V_{jk}|^2 &= \sum_k \langle j| e^{iE_j\tau/\hbar} V |k\rangle e^{-iE_k\tau\hbar} \langle k| V |j\rangle \\
&= \langle j| \underbrace{e^{i\mathcal{H}_0\tau/\hbar} V e^{-i\mathcal{H}_0\tau/\hbar}}_{V(\tau)} V |j\rangle \\
&= \langle j| V(\tau)V(0) |j\rangle
\end{aligned} \tag{2.5}$$

In the semi-classical limit, quantum mechanical expectations correspond to a micro-canonical average. Therefore,

$$\sum_k e^{i(E_j - E_k)\tau/\hbar} |V_{jk}|^2 = \langle V(\tau)V(0)\rangle_j \tag{2.6}$$

where $\langle\cdot\rangle_j$ signifies the micro-canonical average with respect to E_j. Due to the ergodicity implied by the chaoticity of the system, the micro-canonical average is identical to the the time average. In other words,

$$\langle V(\tau)V(0)\rangle = \langle V(\tau + t)V(t)\rangle_t = C_j(\tau) \tag{2.7}$$

where $\langle\cdot\rangle_t$ signifies the time average, and $C_j(\tau)$ is the autocorrelation function. The subscript denotes the micro-canonical averaging over the E_j energy level. In the semi-classical limit, i.e., continuous energy spectrum, the sum $\sum_k$ becomes the integral $\int g(E_k)dE_k$, where the function g is the density of states. So we have,

$$\int e^{i(E_j-E_k)\tau/\hbar}|V_{E_j,E_k}|^2 g(E_k)dE_k = C_j(\tau). \tag{2.8}$$

The left hand side has the form of a Fourier transform. The relationship between the autocorrelation function and the power spectrum, $\tilde{C}(\omega)$, is:

$$\frac{1}{2\pi}\int e^{i\omega\tau}\tilde{C}(\omega)d\omega = C(\tau). \tag{2.9}$$

This establishes the validity of Equation (2.4).

There are many examples that show the validity and usefulness of Equation (2.4). Cohen and Kottos [23] demonstrate its validity in describing accurately a particle trapped in a 2D well. The system is described by some parametric Hamiltonian $\mathcal{H}(Q,P;x)$ where (Q,P) are canonical coordinates, and x is a parameter. In the example under consideration,

$$\mathcal{H} = \frac{1}{2}(P_1^2 + P_2^2 + Q_1^2 + Q_2^2) + xQ_1^2Q_2^2. \tag{2.10}$$

The classical dynamics of this Hamiltonian has a chaotic regime. The particle is evolved in the chaotic regime far in time. The Poincaré plot was checked to ensure the trajectory covered the phase space ergodically. From the description of the

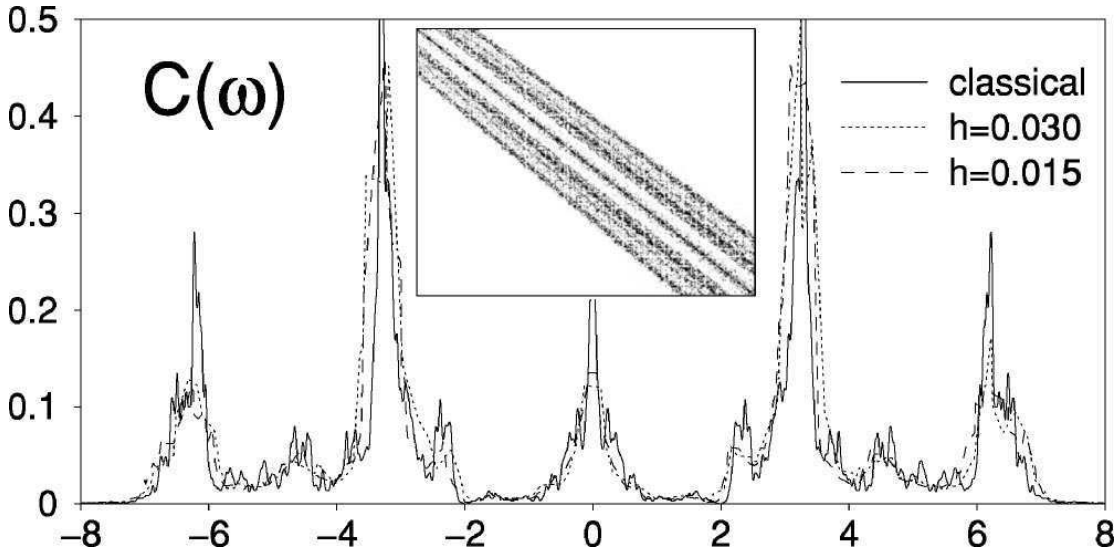

Figure 2.2: The power spectrum inferred from the classical dynamics is plotted with the power spectrum inferred from the matrix elements of the matrix elements of the perturbation operator of the quantized Hamiltonian. The inset is a representative random matrix. Taken from [23].

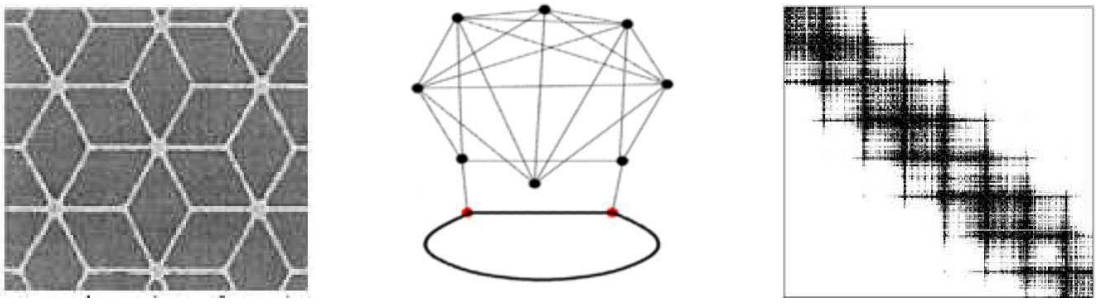

Figure 2.3: *(left)* The geometry of the 2D wires used in the experiment [24] *(center)* the network theoretic representation of the problem from [25] *(right)* an example random matrix corresponding to the network theory model [25].

Hamiltonian, it follows that the generalized force is given by,

$$\mathcal{F} = -\frac{\partial \mathcal{H}}{\partial x} = -Q_1^2 Q_2^2. \tag{2.11}$$

So then the autocorrelation function and power spectrum can be computed for this particular trajectory. Since the trajectory covers phase space ergodically, this autocorrelation function and power spectrum ought to be the same for any similar trajectory. The next step is to quantize the Hamiltonian. It has a straightforward representation in the basis $\mathcal{H}(Q, P; 0)$, but we wish to express it in the basis of $\mathcal{H}_0 = \mathcal{H}(Q, P; 1)$. This diagonalization was performed numerically. From this the perturbation matrix can be extracted, and the power spectrum, $\tilde{C}(\omega)$ can be computed. Thus, two techniques can be used to arrive at the power spectrum, and they both should yield the same result. Figure 2.2 shows that both methods produce strikingly similar results.

Another physical setup would be superconductivity in 2D wires. Figure 2.3

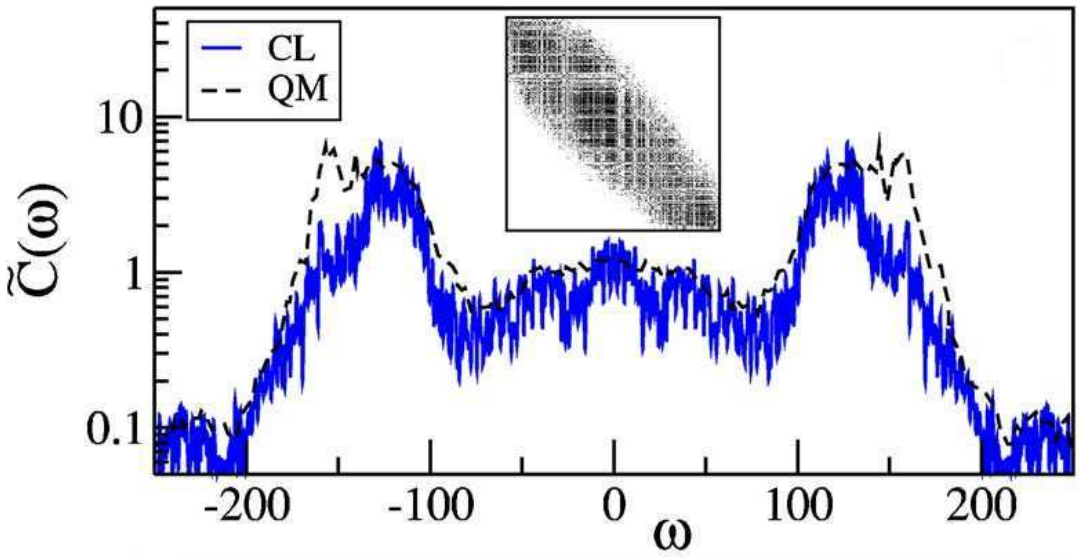

Figure 2.4: Comparison of the power spectrum inferred from the classical dynamics of the BHH [26], and the power spectrum inferred from the matrix elements of the perturbation operator of the quantized problem.

(left) shows a physical setup where a superconductor is allowed to flow through wires defined with the particular geometry described in the figure. This is the experiment described in [24]. The system admits a network model treatment, depicted in Figure 2.3 *(center)*. An example random matrix from such a network model is shown in Figure 2.3 *(right)*.

Hiller, Kottos, and Geisel [26] also provide another example of the use of Equation (2.4) in their study of the Bose-Hubbard Hamiltonians, relevant for the study of Bose-Einstein Condensates. The agreement between the quantum mechanical expression for the power spectrum and the classical expression is shown in Figure 2.4.

In all these examples, we see that generic chaotic systems have perturbation

operators (represented in the basis of the unperturbed Hamiltonian) that posses a finite bandwidth ω_c. This bandwidth is related with the classical correlation time by $\omega_c = 2\pi\hbar/\tau_{\rm cl}$. We will see later on in this thesis that this novel energy scale appearing due to the chaotic nature of the classical dynamics will affect significantly the quantum evolution.

2.2 Conclusion

We have seen that there are many physical systems that can be described with parametric Hamiltonians, and we have developed a semi-classical connection between the classical power spectrum of a generalized force and structured random matrices with a finite band-profile. This motivates the mathematical models that we will investigate in the remainder of this thesis. These models share this generic feature (finite bandwidth) of physical systems. The main assumption that we will adopt is that, due to the complexity of the underlying classical dynamics, the matrix elements of the Hamiltonian matrices can be modeled as independent Gaussian distributed random variables with variance determined by the classical power spectrum. This is operating within the paradigm of RMT proposed by Wigner, who originally proposed ensembles of random matrices as models to describe the statistical properties of the spectra of complex nuclei and atoms.

3 Basic Elements of RMT: Universality in the Eigenvalue and Eigenvector Statistics

The Random Matrix Theory of Hamiltonian systems is based on the assumption that, for complex systems, we know very little about the exact Hamiltonian matrix of the system we are considering except for certain symmetry properties. These symmetry properties impose restrictions on the form of the Hamiltonian matrix. One of the most obvious examples is the requirement that a Hamiltonian operator $\mathcal{H}$, describing a physical system, is in general hermitian $\mathcal{H}^\dagger = \mathcal{H}$ and thus all matrices modeling a Hamiltonian must themselves be hermitian. This ensures that its eigenvalues, the allowed energies of the system, are real. Further symmetry considerations can also exist, and their consideration can significantly simplify the structure of the Hamiltonian matrix. For example a request for a time reversal invariance on the Hamiltonian matrix (and for the case of integer spins) leads to the further requirement that the matrix has to be real symmetric.

Various other considerations can lead to other constrains as far as the matrix elements of the Hamiltonian matrix are concerned. In this section, we will focus on the RMT modeling of these two types, i.e., Hamiltonian matrices that are hermitian or real symmetric. The main assumption underlying the RMT paradigm is that the elements of the Hamiltonian matrix are themselves independent random variables. Given this assumption, we can then determine their probability distribution by requiring that the information contained in the random Hamiltonian matrix is minimal [5]. This leads to a Gaussian distribution for matrix elements. The resulting RMT ensembles that describe complex hermitian or real symmetric matrices are called the Gaussian Unitary Ensemble (GUE) and the Gaussian Orthogonal Ensemble (GOE), respectively. One of their main properties is their invariance under unitary or orthogonal transformations, respectively. Our main interest in this chapter is to investigate the statistical properties of their corresponding eigenvalues and eigenvectors.

3.1 Unfolding the Spectra

Before we can discuss any results of RMT, it is necessary to briefly mention a procedure that is always performed in RMT calculations in order to make the predictions of RMT comparable with a physical situation. The important point to keep in mind is that RMT predictions are always about the fluctuations around an average, but they are insensitive to what that average actually is. The average arises due to the particulars of the system, which is necessarily a non-universal. This non-universality is removed from the analysis by the process of **unfolding**

the spectra. This topic is described in detail in Bohigas [27]. We describe this process for an arbitrary hermitian matrix, $\mathcal{H}$, coming from some collection of random matrices H. Because $\mathcal{H}$ is hermitian, it has real eigenvalues. Let us order them in the following way:

$$E_1 \leq E_2 \leq \cdots \leq E_k \leq \cdots . \tag{3.1}$$

We can define the staircase or counting function, $N(E)$ to count the number of eigenvalues less than or equal to E. The collection H defines some $\langle N^{\mathcal{H}}(E) \rangle$, where the brackets denote averaging over all members of the system H. So then we can write,

$$N^{\mathcal{H}}(E) = \underbrace{\langle N^{\mathcal{H}}(E) \rangle}_{\text{smooth term}} + \underbrace{\delta N^{\mathcal{H}}(E)}_{\text{fluctuating term}} \tag{3.2}$$

The smooth term is system dependent (non-universal). We wish to transform the eigenvalues of $\mathcal{H}$ in such a way that the smooth term becomes trivial. This is done through the transformation that sends the energies $\{E_1, E_2, \ldots\}$ to $\{x_1, x_2, \ldots\}$ by,

$$E_k \mapsto \langle N^{\mathcal{H}}(E_k) \rangle = x_k. \tag{3.3}$$

The new collection of unfolded energies $\{x_1, x_2, \ldots\}$ has a trivial smooth term. Namely,

$$\langle N^*(x) \rangle = x. \tag{3.4}$$

And thus $\{x_1, x_2, \ldots\}$ all have an average separation of one. In other words, the mean level spacing, Δ, of the new collection of eigenvalues is unity.

3.2 Eigenvalue Statistics

The simplest and most frequently used measure of the complexity of a quantum system in the field of quantum chaos is the level spacing distribution. This statistical measure captures the sub-$\hbar$ features of the energy spectrum that are **universal** and follow RMT predictions. It is important to understand what the universal features are, because one of the objectives in this thesis is to draw attention to the importance of non-universal (system specific) features that affect the response and quantum dynamics. Theses non-universal features are "fingerprints" of the underlying classical dynamics. Following the original thinking of Wigner, the presentation below will only consider 2×2 random matrices. Pedagogically, this is the most effective approach to understand the origin of correlations in the spectrum of RMT models, and the predictions very accurately correspond to the general $N \times N$ case.

The relevant eigenvalue statistic will be the **nearest neighbor level spacing**. Define the nearest neighbor spacing for the n^{th} level of some Hamiltonian $\mathcal{H}$ to

be,

$$S_n = \frac{E_n - E_{n-1}}{\Delta} \tag{3.5}$$

where Δ is the mean level spacing. Since we assume that the spectra has been unfolded, we can say that $\Delta = 1$. Thus the nearest neighbor level spacing is simply denoted by S. The nearest neighbor level spacing distribution measures the probability that there are no eigen-energies distance s away from a fixed eigen-energy, and also simultaneously that there is an eigen-energy in the region $[s, s+ds]$. We now restrict the derivation to 2×2 matrices in the GOE and GUE. This result, surprisingly, differs only slightly from the arbitrary $N \times N$ case[1].

Let $\mathcal{H}$ be a Hamiltonian. So then

$$\mathcal{H} = \begin{pmatrix} H_{11} & H_{12} \\ H_{12}^* & H_{22} \end{pmatrix} = \begin{pmatrix} A & X + iY \\ X - iY & B \end{pmatrix} \tag{3.6}$$

where A, B, X and Y are real numbers. Following the principles of RMT, we will treat them as random variables. In the GOE case, $\mathcal{H}$ must be real symmetric, so $Y = 0$. For the GUE case, there is no restriction on Y. Since $\mathcal{H}$ is a 2×2 matrix, it can have at most two eigenvalues. So there is just one nearest neighbor, and call its spacing S.

We can compute S from the eigenvalues of $\mathcal{H}$. By definition, this is:

$$S = E_2 - E_1 \tag{3.7}$$

[1]See [2] pp. 64-69 for GOE case, and p. 78 for GUE.

where E_1 and E_2 are the eigenvalues of $\mathcal{H}$. It is straightforward to show that,

$$S = \sqrt{W^2 + X^2 + Y^2} \tag{3.8}$$

where $W = B - A$. For real symmetric $\mathcal{H}$, we have that $Y = 0$. Next, we can assume that X is a Gaussian random variable with mean $\mu = 0$ and standard deviation σ. Furthermore, we assume that A and B are Gaussian random variables with mean $\mu = 0$ and standard deviation $\sigma/\sqrt{2}$. Thus W is a Gaussian with mean $\mu = 0$ and standard deviation σ, by a property of sums of Gaussians. The problem is to compute $f_S(s)$, the probability density function of S, where S is a function of the random variables X and W. Since X and W are independent random variables, we can write that:

$$f_S(s) \propto \iint \delta(s - \sqrt{w^2 + x^2})\ e^{-(x^2+w^2)/(2\sigma^2)} dx dw \tag{3.9}$$

This integration is easily performed in polar coordinates ($r^2 = x^2 + y^2$):

$$\begin{aligned} f_S(s) &\propto \iint \delta(s - r) e^{-r^2/(2\sigma^2)} r dr d\theta \propto \int \delta(s - r) e^{-r^2/(2\sigma^2)} r dr \\ &\propto s e^{-s^2/(2\sigma^2)} \end{aligned} \tag{3.10}$$

Integration over all s will determine the normalization condition. Next, we consider the GUE case. In the GUE case there is no longer the restriction that $Y = 0$. Instead Y is also a Gaussian random variable with mean $\mu = 0$ and

standard deviation σ. So then,

$$f_S(s) \propto \iiint \delta(s - \sqrt{w^2 + x^2 + y^2})\ e^{-(w^2+x^2+y^2)/(2\sigma^2)} dwdxdy. \tag{3.11}$$

This integration is easily performed in spherical coordinates ($r^2 = w^2 + x^2 + y^2$). We use the convention that the Jacobian is $r^2 \sin\theta$.

$$\begin{aligned} f_S(s) &\propto \iiint \delta(s - r)\ e^{-r^2/(2\sigma^2)} r^2 \sin\theta dr d\theta d\phi \\ &\propto s^2 e^{-s^2/(2\sigma^2)} \end{aligned} \tag{3.12}$$

For the sake of comparison, we will now derive the nearest neighbor spacing distribution for an integrable system. This is done more rigorously in Berry [28]. For the integrable case, the eigen-energies are uncorrelated random variables, i.e., the Hamiltonian is a diagonal matrix where the diagonal elements are uncorrelated random variables. Without loss of generality, say that this region of unfolded spectra is an energy window $[0, A]$, with N levels in this region. We will eventually take $N \to \infty$. We will now compute $f_S(s)ds$ by directly computing the probability that there is gap of length s in the region $[0, A]$ with no eigen-energies, and multiplying that by the probability of finding an eigen-energy in the region $[s, s + ds]$.

The first step is to compute the probability that there are no eigen-energies in the region $[0, s]$. For a single eigen-energy, the probability that it is in the region $[0, s]$ is s/A, because each eigen-energy is assumed to be uniformly distributed. So the probability of not being in the region is $1 - s/A$. The probability for N

levels like this to not be in the region is thus $(1 - s/A)^N$. We can express A in terms of the number of sites, N, and the mean level spacing, $\Delta = 1$, by $A = N\Delta$. So taking the $N \to \infty$ limit, we have that:

$$P(\text{no eigen-energies between } [0, s]) = \lim_{N\to\infty} \left(1 - \frac{s}{N}\right)^N = e^{-s} \tag{3.13}$$

This is almost what we are looking to compute, but the nearest neighbor level spacing is the probability of finding no eigen-energy in $[0, s]$ and the probability of finding an eigen-energy in the space $[s, s+ds]$. We have computed the former. We argue that the latter is simply some constant multiplied by ds. It is not necessary to specify what the constant is, because it can be determined by normalizing the probability distribution. The important point is that this value does not depend on s, which is reasonable because the uniform distribution of the eigen-energies. So then we can conclude that the nearest neighbor spacing is,

$$f_S(s)ds = e^{-s} \times kds = e^{-s}ds \tag{3.14}$$

where $k = 1$ by normalization. Therefore $f_S(s) = e^{-s}$.

The results from above can be summarized as follows:

$$f_S(s) \propto \begin{cases} s^0 e^{-s} & \text{integrable systems} \\ s^1 e^{-s^2/(2\sigma^2)} & \text{GOE} \\ s^2 e^{-s^2/(2\sigma^2)} & \text{GUE} \end{cases} \tag{3.15}$$

Figure 3.1 plots these various distributions. For small values of s, s^n dominates

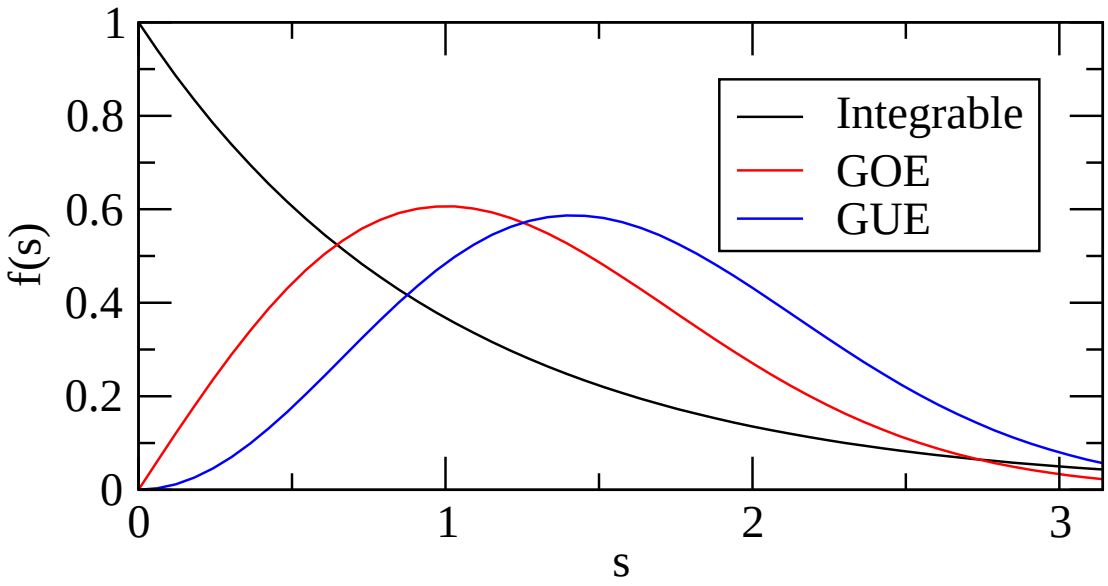

Figure 3.1: Level spacing distributions for the three classes of systems considered. The behavior near the origins clearly shows the level repulsion of chaotic systems.

the exponential. So the ensemble determines how strongly adjacent levels repel each other. The way to understand this is by observing that the GUE involves more uncorrelated random variables compared with the GOE. This means that near by spacings are less likely because it is more rare for the random variables to be arranged in the required way to get near by level spacings.

3.3 The n-Level Correlator, Cluster Function and Form Factor

In the last section, we found that energy level repulsion is an important feature of the chaoticity of a system (i.e., integrable motion experienced no level repulsion, but chaotic motion did). Following this observation, we define several distributions that probe the clustering of levels. These will be useful later on in Section 4.1.4 when we consider the decay of a bound state into a sea of states with energy levels drawn from a Gaussian ensemble.

We begin by defining a multivariate probability density function for the eigenvalues of an ensemble of random $N \times N$ matrices H. Call such a p.d.f. $p_H(x_1, \ldots, dx_N)$, where $p_H(x_1, \ldots, dx_N)dx_1 \cdots dx_N$ is the probability of finding the eigenvalues of a representative in the ensemble to be in the interval $[x_1, x_1 + dx_1] \times \cdots \times [x_N, x_N + dx_N]$. Note that such a definition undercounts the description of the eigenvalues because it is sensitive to the order they appear. For example, if H is a 2×2 ensemble, then the probability of getting eigenvalues $\{a, b\}$ is evenly split between the quantities $p_H(a, b)dx_1dx_2$ and $p_H(b, a)dx_1dx_2$. A more relevant quantity will

be insensitive to indexing, i.e., (a, b) should be the same as (b, a). This is accomplished by a combinatorial factor that appears before the integral in the next definition. The next step to understand level clusterings is to define a quantity that characterizes the probability of finding n eigenvalues $\{x_1, \ldots, x_n\}$ irrespective of indexing and placing no restrictions on the other eigenvalues. This is the marginal probability density function of n variables of $p_H(x_1, \ldots, x_N)$ multiplied by a combinatorial factor to make the probability insensitive to labeling. This is called the **n-level correlation function**, and it is written:

$$R_n(x_1, \ldots, x_n) = \frac{N!}{(N-n)!} \int \cdots \int p_H(x_1, \ldots, x_N) dx_{n+1} \cdots dx_N \tag{3.16}$$

From here we go to a quantity that further emphasizes the clustering of levels, called the **n-point cluster function**. Although there is a general description for all n of them, we only need to understand 2-point cluster function. This is given by,

$$T_2(x_1, x_2) = R_1(x_1)R_2(x_2) - R_2(x_1, x_2). \tag{3.17}$$

The $N \to \infty$ limit of $T_2(x_1, x_2)$ with unfolded spectra is written $Y_2(x_1, x_2)$. It can be shown that Y has the property that it only depends on the quantity $r = |x_1 - x_2|$. The **two-level form factor** is defined to be the Fourier transform of $Y_2(r)$.

$$b(k) = \int e^{2\pi i k r} Y_2(r) dr \tag{3.18}$$

This quantity will be essential to the understanding the revivals of the decay into a sea of discrete states. In particular, we will need the form factor for which ever ensemble the sea of states is described by. The form factor for the GOE is given by[2]

$$b(k) = \begin{cases} 1 - 2|k| + |k| \ln(1 + 2|k|) & |k| < 1 \\ -1 + |k| \ln\left(\frac{2|k|+1}{2|k|-1}\right) & |k| \geq 1 \end{cases} \tag{3.19}$$

For the GUE, we have,

$$b(k) = \begin{cases} 1 - |k| & |k| < 1 \\ 0 & |k| \geq 1 \end{cases} \tag{3.20}$$

These are plotted in Figure 3.2.

3.4 Eigenvector Statistics

The eigenvalue statistics are the first step towards an understanding of the dynamics. The next (more demanding) step is to understand the statistical properties of the eigenstates. Here we present an analysis of the distribution of their components based on the so-called random wave approximation, first promoted by Berry [29]. The derivation below is found in [3].

Let $\vec{\Psi} = (\Psi_1, \Psi_2, \ldots, \Psi_n)$ be an eigenvector of a random matrix. We wish to compute the probability density function of each component, $f_{\Psi_j}(x)$ where

[2]See Mehta [2] pp. 59-61 for GOE and pp. 75-77 for GUE.

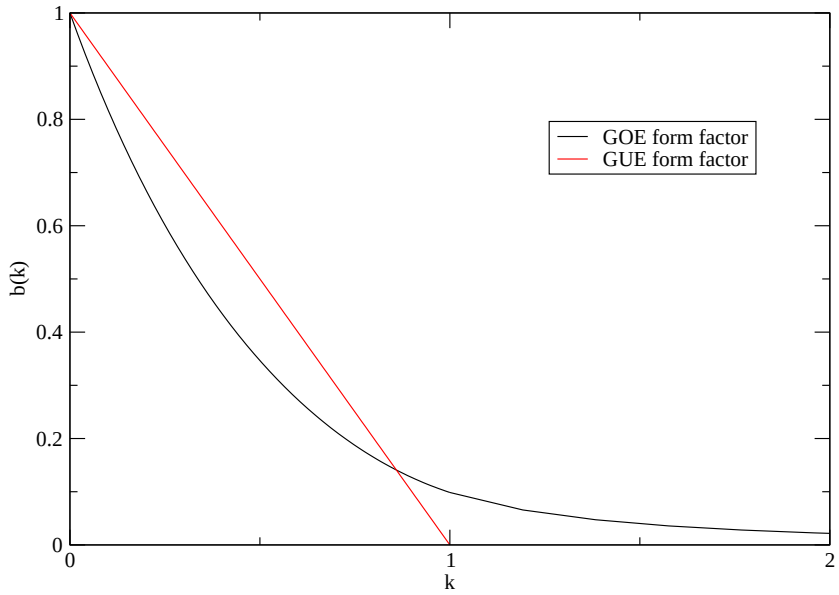

Figure 3.2: Plots of the form factor for the GOE and GUE cases (Equations (3.19) and (3.20)).

$j = 1, \ldots, n$. By symmetry, each Ψ_j should be independent of j, so we will call the quantity we are computing simply $f_\Psi(x)$. We will now derive the result for the GOE case, and show how the argument is easily modified to apply to the GUE case. The ansatz is that the eigenvectors of a random matrix are a superposition of random plane waves. So in position space we have,

$$\Psi(\vec{r}) = \sum_n a_n \cos(k_n \vec{r} - \phi_n) \tag{3.21}$$

where each k_n is a random unit vector, each ϕ_n is a random phase, and a_n are random amplitudes. Note that in the GUE case, a_n would be a random complex number.

We wish to calculate,

$$f_\Psi(x) = \left\langle \delta\left(x - \sum_n a_n \cos(k_n \vec{r} - \phi_n)\right)\right\rangle \tag{3.22}$$

where $\langle\cdot\rangle$ denotes averaging over all phases, amplitudes, and directions. We can write the delta function by a Fourier expression, leading to,

$$f_\Psi(x) = \frac{1}{2\pi}\int e^{ixt}\prod_{n=1}^{N}\left\langle e^{-ita_n\cos(k_n\vec{r}-\phi_n)}\right\rangle. \tag{3.23}$$

Using the Taylor expansion of the exponential,

$$\left\langle e^{-ita_n\cos(k_n\vec{r}-\phi_n)}\right\rangle = 1 - it\left\langle a_n\cos(k_n\vec{r}-\phi_n)\right\rangle - \frac{t^2}{2}\left\langle a_n^2\cos^2(k_n\vec{r}-\phi_n)\right\rangle + \cdots$$

We have that $\langle a_n\cos(k_n\vec{r}-\phi_n)\rangle = 0$ because every positive contribution has an associated negative contribution of the same magnitude. On the other hand, $\langle a_n^2\cos^2(k_n\vec{r}-\phi_n)\rangle = \langle a_n^2\rangle/2$. This is because,

$$a^2\cos^2\theta + a^2\sin^2\theta = a^2 \implies \left\langle a^2\cos^2\theta\right\rangle + \left\langle a^2\sin^2\theta\right\rangle = \left\langle a^2\right\rangle. \tag{3.24}$$

At the same time, due to symmetry, $\langle a^2\cos^2\theta\rangle = \langle a^2\sin^2\theta\rangle$, so $\langle a^2\cos^2\theta\rangle = \langle a^2\rangle/2$. Putting this all together, we can conclude

$$\left\langle e^{-ita_n\cos(k_n\vec{r})-\phi_n}\right\rangle = 1 - \frac{t^2}{4}\left\langle a_n^2\right\rangle + \cdots. \tag{3.25}$$

We can then use the normalization of $\Psi(r)$ to come up with an expression for

$\langle a_n^2 \rangle$.

$$\begin{aligned} 1 &= \int |\Psi(\vec{r})|^2 dA \\ &= \sum_{n,m} \int a_n^\dagger a_m \cos(k_n \vec{r} - \phi_n) \cos(k_m \vec{r} - \phi_m) dA \end{aligned} \tag{3.26}$$

But by the orthonormal properties of the cosine, the integral only contributes a nonzero value just in case $n = m$, and then the contribution is $1/2$. Thus,

$$1 = \frac{A}{2} \sum_{n,m} a_n^\dagger a_m \delta_{n,m} = \frac{A}{2} \sum_n a_n^2. \tag{3.27}$$

If we were modify the argument to address the GUE case, we would find that instead that $(A/2) \sum_n (\mathrm{Re}\,[a_n]^2 + \mathrm{Im}\,[a_n]^2) = 1$. But continuing in the GOE case, we have,

$$\left\langle a_n^2 \right\rangle = \frac{2}{AN} \tag{3.28}$$

where N is the number of waves contributing to the original superposition Ψ. For the GUE case, we can say that $\left\langle \mathrm{Re}\,[a_n]^2 \right\rangle = \left\langle \mathrm{Im}\,[a_n]^2 \right\rangle$, and then Equation (3.28) simply needs to be adjusted by a factor of two. This factor of two will persist throughout the remainder of the argument in the GUE case. So backing up, we can write,

$$\left\langle e^{-ita_n \cos(k_n \vec{r} - \phi_n)} \right\rangle = 1 - \frac{t^2}{2AN} + \cdots \tag{3.29}$$

This is just one factor in a product, but the other factors are identical, so we really have N copies of the above. We are interested in the limit as $N \to \infty$. So we have:

$$\lim_{N\to\infty} \prod_{n=1}^{N} \left\langle e^{-ita_n \cos(k_n \vec{r} - \phi_n)} \right\rangle = \lim_{N\to\infty} \left(1 - \frac{t^2}{2AN} + \cdots\right)^N = e^{\frac{-t^2}{2A}} \tag{3.30}$$

So finally, for the GOE:

$$\begin{aligned} f_\Psi(x) &\propto \int e^{ixt} e^{\frac{-t^2}{2A}} dt \\ &\propto e^{-Ax^2/2} \end{aligned} \tag{3.31}$$

where the proportionality is determined by normalization. Similarly, the GUE result only differs by a factor of two as argued above. Thus the GUE result is,

$$f_\Psi(x) \propto e^{-Ax^2/4} \tag{3.32}$$

where again the proportionality is determined by normalization. This is shown to be in agreement with the numerics shown in Figure 3.3. The deviations are due to "scarring," which has been extensively studied by Heller [8].

3.5 Conclusion

In this chapter we have discussed the predictions of RMT for the distribution of level spacings and the wavefunction components. We began by describing the procedure of unfolding the spectra, which is a method that removes some of the

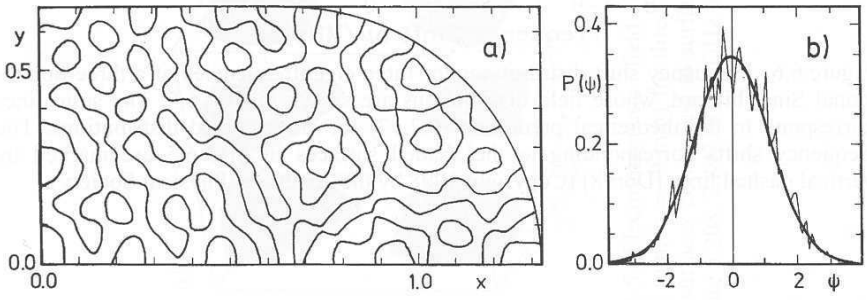

Figure 3.3: The nodal lines of a typical eigenfunction in a quarter stadium (a) and amplitude distribution for the same eigenfunction (b). Reproduced from [3].

non-universal system-specific features of the eigenvalue distribution, in order to allow for a study of universal fluctuations. With this as a foundation, we went on to compute various statistical measures about the eigenvalues and eigenvectors. We found that chaotic systems have levels that repel each other in contrast with integrable systems, which do not. The significance of level repulsion led to defining various eigenvalue correlation functions, though we will not use them in earnest until the next chapter.

4 Wave-Packet Dynamics in Energy Space: The Flat Continuum

This chapter considers the problem of the decay of a prepared state $|\lambda\rangle$ into a sea of other states $\{|E\rangle\}$. This class of problems has broad applications to atomic, nuclear, and mesoscopic physics. The prepared state is coupled to the other states by some perturbation which will be defined by its power spectrum $\tilde{C}(\omega)$. Because of this coupling, the prepared state will decay into the other states. The primary quantity that we will consider to understand this process is the **survival probability**, defined to be:

$$P(t) = \langle \lambda | \lambda(t) \rangle \tag{4.1}$$

where $|\lambda(t)\rangle$ is the time evolution of the state $|\lambda\rangle$. The most physically relevant situation is where the state $|\lambda\rangle$ is coupled to the collection $\{|E\rangle\}$ in the same way that every element in $\{|E\rangle\}$ is coupled to every other element of $\{|E\rangle\}$. Thus $\tilde{C}(\omega)$ is the power spectrum of every energy level. In this thesis, such a model will be referred to as the Wigner Model (WM). Deriving an expression for the survival

probability of the WM is analytically challenging due to the combinatorics of the problem, i.e., the number of possible ways to make a round trip is vast. Due to this difficulty, a simplified model is used in the hope that it will capture the important features of the WM. This simplified model neglects the coupling within the sea of states. In other words, the state $|\lambda\rangle$ has been "singled out" to be the prepared state by the topology (level connectivity) of the model. This model will be referred to as the Friedrichs Model (FM). The combinatorial difficulties are no longer present in this case because a round trip is easily described by $|\lambda\rangle \rightarrow |E\rangle \rightarrow |\lambda\rangle$ for some state $|E\rangle$. The dynamics of the FM is tractable, and the derivation is presented in Section 4.1. For the FM, we consider two possible scenarios involving the energy levels of $\{|E\rangle\}$. First we will consider the case where the sea of states is a continuum, i.e., we will take the mean level spacing to zero. We find the usual Wigner (Fermi Golden Rule) decay scenario, i.e., the survival probability decays like $e^{-\Gamma t}$ for some Γ, which is proportional to the square of the perturbation strength. After doing this, we will modify the argument slightly to consider the effect of giving the energy levels of $\{|E\rangle\}$ level statistics of ensembles of random matrices. Here the survival probability also decays like $e^{-\Gamma t}$, but the decay is followed by a revival whose shape is determined by the form factor of the ensemble (see Section 3.3).

After understanding the dynamics of the Friedrichs model, we attempt to use the results to make meaningful statements about the WM. We find that there is good agreement between the results in both the time and energy domains. This fact is significant for the analysis that will take place in Chapter 5, where we will

see that this good agreement between the FM and WM depends on the particular choice of $\tilde{C}(\omega)$ considered in this chapter.

4.1 The Friedrichs Model

In this section, we calculate the survival probability of a bound state decaying into the flat continuum. A version of this argument can be found in [30]. This type of presentation has the advantage of illuminating the importance of level statistics of the unperturbed Hamiltonian in the relaxation process of the bound state. We will consider both the continuum limit and also the discrete problem with unperturbed eigen-energies distributed with GOE statistics.

4.1.1 Statement of the Model

The system is prepared in the state $|\lambda\rangle$ at time $t = 0$, where $|\lambda\rangle$ is an eigenstate of some Hamiltonian $\mathcal{H}_0$. At time $t = 0$, a perturbation V is introduced so that the total Hamiltonian $\mathcal{H}$ is $\mathcal{H}_0 + V$. This perturbation V couples the state $|\lambda\rangle$ to the other eigenstates of $\mathcal{H}_0$, but there is no coupling other than this. The power spectrum of the generalized force at the $|\lambda\rangle$ energy level is given by,

$$\tilde{C}_\lambda(\omega) = 2\pi\epsilon^2. \tag{4.2}$$

Following the reasoning of Wigner, we will assume that we can treat the perturbation operator V as a random matrix. In other words, if $|\mu\rangle$ is an eigenstate of

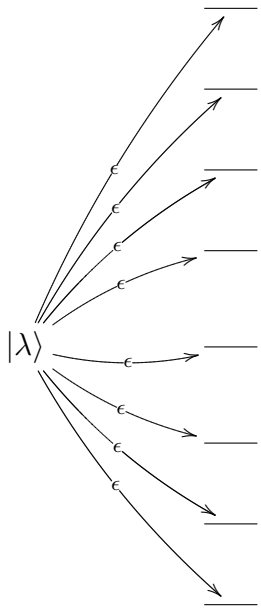

Figure 4.1: Graph theoretic representation of the Friedrich model.

$$\begin{pmatrix}
E_1 & 0 & \cdots & 0 & \epsilon & 0 & 0 & \cdots & 0 \\
0 & E_2 & \cdots & 0 & \epsilon & 0 & 0 & \cdots & 0 \\
0 & 0 & \ddots & \vdots & \vdots & \vdots & \vdots & \ddots & \vdots \\
\vdots & \vdots & & E_{\lambda-1} & \epsilon & 0 & 0 & 0 & 0 \\
\epsilon & \epsilon & \cdots & \epsilon & E_\lambda & \epsilon & \epsilon & \cdots & \epsilon \\
0 & 0 & \vdots & 0 & \epsilon & E_{\lambda+1} & 0 & \cdots & 0 \\
0 & 0 & \vdots & 0 & \epsilon & 0 & E_{\lambda+2} & & \vdots \\
\vdots & \vdots & \ddots & \vdots & \vdots & \vdots & \vdots & \ddots & 0 \\
0 & 0 & \cdots & 0 & \epsilon & 0 & 0 & \cdots & E_N
\end{pmatrix}$$

Figure 4.2: Matrix representation of the Hamiltonian $\mathcal{H}$ written in the basis of $\mathcal{H}_0$. The matrix elements "ϵ" denote random variables of standard deviation ϵ.

$\mathcal{H}_0$, then

$$\langle\lambda|\, V\, |\mu\rangle = \langle\mu|\, V\, |\lambda\rangle = V_{\lambda\mu} \sim N(0, \epsilon^2) \tag{4.3}$$

and if $|\mu'\rangle$ is an eigenstate not equal to $|\mu\rangle$, then

$$\langle\mu|\, V\, |\mu'\rangle = \langle\mu'|\, V\, |\mu\rangle = 0. \tag{4.4}$$

The notation $N(0, \epsilon^2)$ denotes a Gaussian distributed random variable with mean 0 and variance ϵ^2. The latter condition comes from Equation (2.4), which connects the power spectrum and the variance of matrix elements. A schematic representation of this model is depicted in Figure 4.1, and the Hamiltonian $\mathcal{H}$ is shown in Figure 4.2. For the derivation that follows, $|\mu\rangle$ is a representative eigenstate of $\mathcal{H}_0$ (with $|\mu\rangle \neq |\lambda\rangle$), and $|i\rangle$ is a representative state of $\mathcal{H}$. In other words

$$\mathcal{H}_0\, |\mu\rangle = E_\mu^{(0)}; \qquad \mathcal{H}\, |i\rangle = E_i\, |i\rangle\,; \qquad \mathcal{H}_0\, |\lambda\rangle = E_\lambda^{(0)}\, |\lambda\rangle\,.$$

4.1.2 The Local Density of States

Let $|\lambda(t)\rangle$ be the time evolution of the state $|\lambda\rangle$. The objective is to compute the survival probability of the state $|\lambda\rangle$. That is, the quantity: $P(t) = |\langle\lambda|\lambda(t)\rangle|^2$. We observe that[1],

$$|\lambda(t)\rangle = e^{-i\mathcal{H}t}\, |\lambda\rangle = e^{-i\mathcal{H}t} \left(\sum_i |i\rangle\, \langle i| \right) |\lambda\rangle = \sum_i e^{-iE_i t} \langle i|\lambda\rangle\, |i\rangle\,. \tag{4.5}$$

[1]Note that these calculations are performed in units where $\hbar \equiv 1$.

Thus the **survival probability amplitude**, $\alpha(t) = \langle\lambda|\lambda(t)\rangle$, is

$$\alpha(t) = \langle\lambda|\lambda(t)\rangle = \sum_i e^{-iE_i t}\langle\lambda|i\rangle\langle i|\lambda\rangle = \sum_i e^{-iE_i t}|\langle\lambda|i\rangle|^2. \tag{4.6}$$

This shows that the survival probability amplitude is the discrete Fourier transform of $|\langle\lambda|i\rangle|^2$. A quantity that is closely related to $|\langle\lambda|i\rangle|^2$ is called the **Local Density of States** or **LDoS**, and it is defined to be

$$\rho(\omega) = \sum_i |\langle\lambda|i\rangle|^2\delta(\omega - E_i). \tag{4.7}$$

The quantity $|\langle\lambda|i\rangle|^2$ is called the **LDoS kernel**. Thus, the Fourier transform of the LDoS is the survival probability amplitude.

A few words are in order regarding the definition of the LDoS, and its importance in physical applications. The LDoS, also known as the strength function, describes an energy distribution. Conventionally it is defined as follows:

$$\rho(\omega) = -\frac{1}{\pi}\langle\lambda|\,\mathrm{Im}\left[G^+(\omega)\right]|\lambda\rangle \tag{4.8}$$

where $G^+(\omega) = 1/((\omega+i0)\mathbb{1} - \mathcal{H}_0)$ is the retarded Green's function. We show that these definitions are equivalent in Appendix B.1. The LDoS is important in the studies of chaotic or complex conservative quantum systems that are encountered in nuclear physics, as well as in atomic and molecular physics. Related applications may be found in mesoscopic physics. Going from $\mathcal{H}_0$ to $\mathcal{H}$ may signify a physical change of an external field, switching on a perturbation, or a sudden change of an

effective interaction as in molecular dynamics. Here we will present a derivation of the LDoS kernel (occasionally, we will refer to this as the LDoS) for the FM.

Straightforward algebraic manipulation allows us to write a generic state $|i\rangle$ of $\mathcal{H}$ as

$$|i\rangle = \frac{|\lambda\rangle + \sum_{\mu} c_\mu |\mu\rangle}{\sqrt{1 + \sum_{\mu} |c_\mu|^2}}. \tag{4.9}$$

for some collection of c_μ's depending on the state $|i\rangle$ (see Appendix A.1 for details). Given Equation (4.9) and the eigenvalue equation $\mathcal{H}|i\rangle = E_i|i\rangle$, we can conclude that

$$\mathcal{H}[|\lambda\rangle + \sum_{\mu} c_\mu |\mu\rangle] = E_i[|\lambda\rangle + \sum_{\mu} c_\mu |\mu\rangle]. \tag{4.10}$$

Multiplying both sides of this equation by $\langle\lambda|$ and $\langle\mu|$ leads to the following two relations:

$$\langle\lambda|(\mathcal{H}_0 + V)[|\lambda\rangle + \sum_{\mu} c_\mu |\mu\rangle] = \langle\lambda| E_i[|\lambda\rangle + \sum_{\mu} c_\mu |\mu\rangle]$$
$$\therefore E_\lambda^{(0)} + \sum_{\mu} V_{\lambda\mu} c_\mu = E_i \tag{4.11a}$$

$$\langle\mu|(H_0 + V)[|\lambda\rangle + \sum_{\mu} c_\mu |\mu\rangle] = \langle\mu| E_i[|\lambda\rangle + \sum_{\mu} c_\mu |\mu\rangle]$$
$$\therefore V_{\lambda\mu} + E_\mu^{(0)} c_\mu = E_i c_\mu \tag{4.11b}$$

Equation (4.11a) will be used later. Solving Equation (4.11b) for c_μ gives $c_\mu = \frac{V_{\lambda\mu}}{E_i - E_\mu^{(0)}}$. Substituting this into Equation (4.9) gives,

$$|\langle\lambda|i\rangle|^2 = \left(1 + \sum_\mu \left[\frac{|V_{\lambda\mu}|}{E_i - E_\mu^{(0)}}\right]^2\right)^{-1} \tag{4.12}$$

This expression is true for all possible $V_{\lambda\mu}$'s and $E_\mu^{(0)}$'s. We will compute the average LDoS kernel of the ensemble, which is given by

$$\left\langle |\langle\lambda|i\rangle|^2 \right\rangle = \left\langle \left(1 + \sum_\mu \left[\frac{|V_{\lambda\mu}|}{E_i - E_\mu^{(0)}}\right]^2\right)^{-1} \right\rangle \tag{4.13}$$

By properties of the expectation value of independent random variables, we are free to replace every $\langle |V_{\lambda\mu}|^2 \rangle$ with ϵ^2. To approach the continuum, we will assume that the energies of the unperturbed Hamiltonian follow a picket fence distribution with mean level spacing Δ. Eventually we will take the limit as Δ approaches zero. The picket fence distribution means that the unperturbed energies are of the form $E_\mu^{(0)} = E_\lambda^{(0)} + \Delta \cdot \mu$ where μ is an integer. Leaving to the Appendix A.2 the technical details, we write below the final expression for the LDoS:

$$|\langle\lambda|i\rangle|^2 = \frac{\epsilon^2}{(\Gamma/2)^2 + (E_\lambda^{(0)} - E_i)^2}. \tag{4.14}$$

where

$$\Gamma = \frac{2\pi\epsilon^2}{\Delta}\sqrt{1 + \left(\frac{\Delta}{\pi\epsilon}\right)^2}.$$

4.1.3 The Continuum Limit

The next step is to take the continuum limit. This means taking the limit as Δ approaches zero, but this condition is not strong enough. If we naively set $\Delta \to 0$, then the quantity Γ would diverge, and the LDoS would be meaningless. In order for this to not happen, we must take the limit carefully. In particular, we must write,

$$\lim_{\Delta \to 0} \Gamma\Delta = \text{const.} \tag{4.15}$$

This will ensure that Γ does not blow up in the continuum limit. In this limit, we find that,

$$\Gamma = 2\pi \frac{\epsilon^2}{\Delta} \tag{4.16}$$

Thus the expression for the LDoS kernel is,

$$|\langle \lambda | i \rangle|^2 = \frac{1}{\pi} \frac{(\Gamma/2)\Delta}{(\Gamma/2)^2 + (E_\lambda^{(0)} - E_i)^2}. \tag{4.17}$$

We have been discussing the LDoS kernel all the time, but now we will discuss the LDoS itself:

$$\rho(\omega) = \sum_i |\langle \lambda | i \rangle|^2 \delta(\omega - E_i). \tag{4.18}$$

In the continuum limit,

$$\sum_i \mapsto \int \frac{d\omega'}{\Delta}.$$

Therefore we can conclude that in the continuum limit, the LDoS is,

$$\rho(\omega) = \int_{-\infty}^{\infty} \frac{1}{\pi} \frac{(\Gamma/2)\cancel{\Delta}}{(\Gamma/2)^2 + (E_\lambda^{(0)} - \omega')^2} \delta(\omega - E_{\omega'}) \, \frac{d\omega'}{\cancel{\Delta}}. \tag{4.19}$$

Lastly, we arrive at our final expression for the LDoS,

$$\rho(\omega) = \frac{1}{\pi} \frac{(\Gamma/2)}{(\Gamma/2)^2 + (E_\lambda^{(0)} - \omega)^2}, \tag{4.20}$$

which is a Lorentzian. Recall that the Fourier transform of LDoS is the survival probability amplitude. Thus, the survival probability amplitude is $\alpha(t) = e^{-\Gamma t/2}$, and substituting into the definition of the survival probability, we conclude that

$$P(t) = |\alpha(t)|^2 = e^{-\Gamma t}. \tag{4.21}$$

Figure 4.3 shows the results of a numerical simulation of the model under consideration. The simulations were performed by numerical integration of the Shrödinger equation in a Hilbert space of size N. The ensemble consisted of 100 random matrices with the structure described as above. We observe that there is good agreement with the theory with respect to the functional form (exponential decay) as well as the scaling parameter $(1/\Gamma)$. Note that in these simulations, and all others using this simulator, $\Delta = 1$.

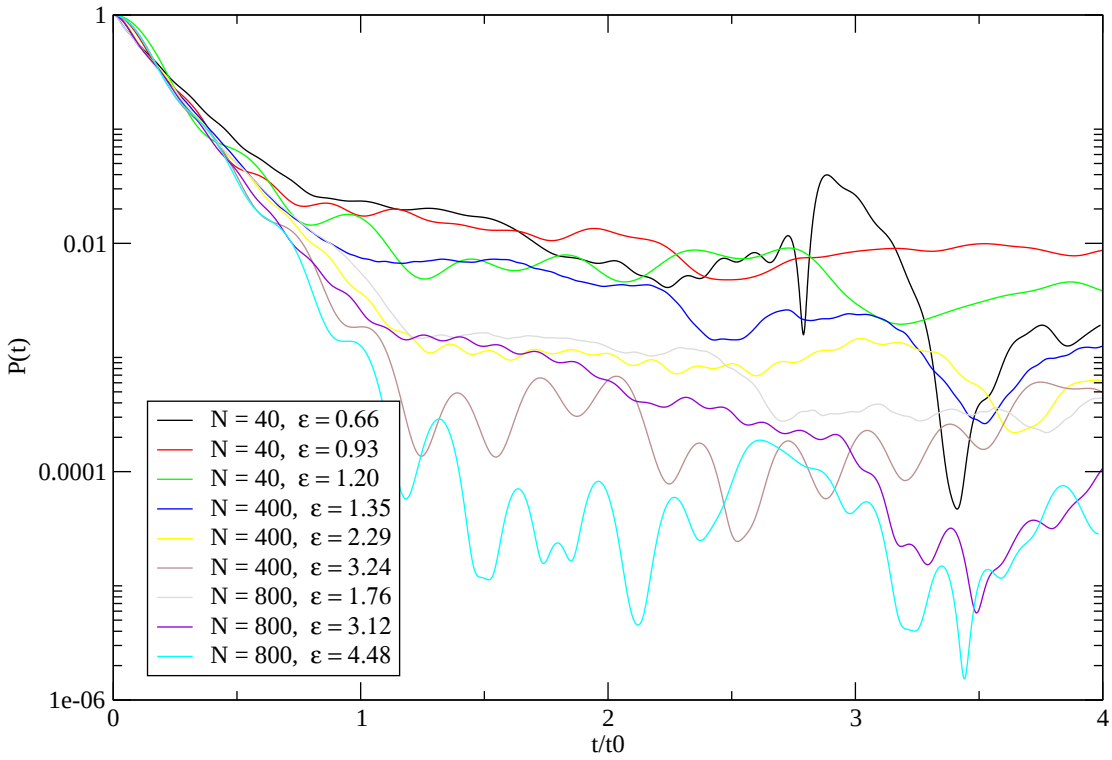

Figure 4.3: Survival probability for various perturbation strengths with scaled time $t_0 = 1/\Gamma$.

4.1.4 Energy Distributions

Rather than taking a picket fence energy distribution in the continuum limit, it is possible to use the argument above to study the importance of discreteness and level distributions on the dynamics of the system. We will suppose that the unperturbed energies of $\mathcal{H}_0$ come from some RMT ensemble. This argument follows closely the argument presented by Mello, *et al.* [31]. We begin by writing the kernel of the LDoS as the sum of a smooth and fluctuating component. This is reminiscent of the procedure used to unfold the spectra. That is to say,

$$|\langle i|\lambda\rangle|^2 = w(E_i) + \delta w_i \tag{4.22}$$

where $w(E_i)$ is the smooth part and δw_i represents the fluctuations about the smooth part. Because the LDoS kernel is normalized, it follows that,

$$\sum_i w(E_i) + \sum_i \delta w_i = 1 \tag{4.23}$$

A quantity that will be useful for this analysis is

$$W = \sum_i w(E_i). \tag{4.24}$$

Such a quantity is called a **linear statistic**, and there exists some mathematical machinery for dealing with linear statistics. In particular, we will be looking to compute their variance. What we will show is that we can express the survival probability in terms of a linear statistic, like the one defined above. This is

because,

$$\begin{aligned} P(t) &= \sum_{i,j} w_i w_j e^{i(E_j - E_i)t} \\ &= \sum_{i,j} (w(E_i) + \delta w_i)(w(E_j) + \delta w_j) e^{i(E_j - E_i)t}. \\ &\approx \left(\sum_i w(E_i) e^{-E_i t} \right)^2 \end{aligned} \tag{4.25}$$

and $\sum_i w(E_i)e^{-E_i t} = \sum_i w_t(E_i)$ is a linear statistic. Call this $\alpha(t)$, which is the survival probability amplitude. Now the variance of $\alpha(t)$ is

$$\left\langle \alpha^\dagger(t)\alpha(t) \right\rangle - \left\langle \alpha(t) \right\rangle \left\langle \alpha^\dagger(t) \right\rangle \tag{4.26}$$

We will not prove it here[2], but it can be shown that this variance is given by,

$$\frac{1}{\Delta} \int_{-\infty}^{\infty} |\phi_t(\tau)|^2 [1 - b(\Delta\tau)] d\tau \tag{4.27}$$

where $\phi_t(\tau)$ is the Fourier transform of $w_t(E)$,

$$\begin{aligned} \phi_t(\tau) &= \int w_t(E) e^{-2\pi i E\tau} dE \\ &= \int w(E) e^{-2\pi i E(\tau + t/(2\pi))}. \end{aligned} \tag{4.28}$$

and $b(k)$ is the form factor discussed in Section 3.3. So if we can determine $\langle \alpha(t) \rangle$, then we will have succeeded to derive an expression for $P(t)$. We can approximate

[2]See [32] for details.

such an expression for $\langle\alpha(t)\rangle$ by passing from discrete to continuous levels.

$$\begin{aligned}\langle\alpha(t)\rangle &= \sum_i \left\langle w(E_i) + \delta w_i e^{-iE_i t}\right\rangle = \sum_i \left\langle w(E_i) e^{-iE_i t}\right\rangle \\ &= N\int w(E_i)e^{-iE_i t}p(E_i)dE_i = N\int_L w(E)e^{-iEt}\frac{dE}{L} \\ &= \frac{1}{\Delta}\int w(E)e^{-iEt}dE \end{aligned} \tag{4.29}$$

where Δ is the mean level spacing, and $p(E_i)$ is the probability density. So then $\langle\alpha(t)\rangle$ is given by the same argument for the picket fence energy distribution given early in the chapter, and so

$$\langle\alpha(t)\rangle = e^{-\Gamma t/2}. \tag{4.30}$$

We can conclude that

$$\begin{aligned}\langle P(t)\rangle &= \left\langle \alpha(t)\alpha^\dagger(t)\right\rangle \\ &= \langle\alpha(t)\rangle\left\langle\alpha^\dagger(t)\right\rangle + \frac{1}{\Delta}\int_{-\infty}^{\infty}|\phi_t(\tau)|^2[1-b(\Delta\tau)]d\tau \\ &= e^{-\Gamma t} + \frac{1}{\Delta}\int_{-\infty}^{\infty}|\phi_t(\tau)|^2[1-b(\Delta\tau)]d\tau. \end{aligned} \tag{4.31}$$

This result is plotted along with a numerical simulation for the GOE case in Figure 4.4. The decay clearly follows an exponential decay followed by a strong revival, which is unrelated to the trivial Heisenberg time recurrences. This demonstrates the importance of level statistics in the wave-packet dynamics. Furthermore, another significant point this analysis raises is the importance of the averaging

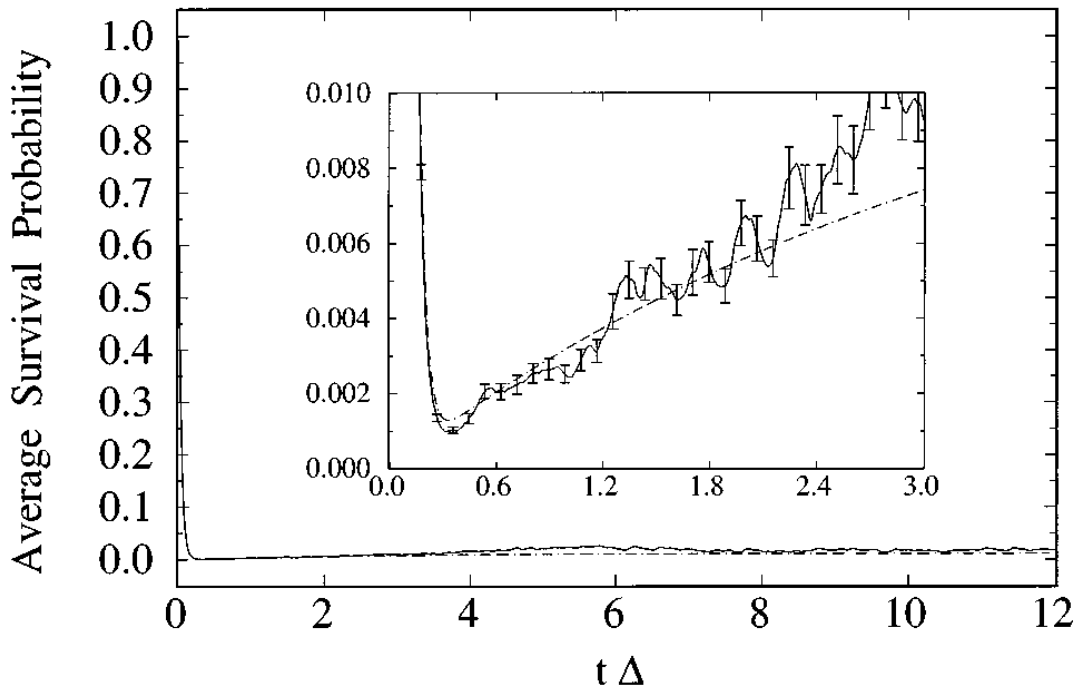

Figure 4.4: Average survival probability from numerical simulations compared with the theoretical expression. Reproduced from [31]. The time axis is in units of the Heisenberg time, so it is clear that the revival is not due to the trivial recurrences.

methods for computing the average $P(t)$. In general, it is not true that,

$$\left\langle |\alpha(t)|^2 \right\rangle = |\left\langle \alpha(t) \right\rangle|^2. \tag{4.32}$$

This is clearly shown in this case, because we explicitly calculate both quantities, and they are surely different. In fact, their difference is governed by the form factor.

4.2 Wigner Banded Random Matrix Model (WM)

We will study a system described by a Hamiltonian $\mathcal{H} = \mathcal{H}_0 + \delta x V$ where $\mathcal{H}_0$ is a diagonal matrix with the picket fence distribution and mean level spacing Δ, and V is a banded random matrix of with random matrix elements of constant variance σ within some band $0 < |n - m| \leq b$. Outside the band, the matrix elements are strictly zero. We will say that $\sigma = 1$, and control the strength of the perturbation exclusively through δx. The model is completely determined by the parameters $(\Delta, b, \delta x, \hbar)$. The system is prepared in state $|\lambda\rangle$ at time $t = 0$, where $|\lambda\rangle$ is an eigenvector of the unperturbed Hamiltonian in the middle of the spectrum. Without loss of generality, say that $|\lambda\rangle$ has unperturbed energy 0. The state $|\lambda\rangle$ then evolves in $\mathcal{H}$ for $t > 0$.

We can define several other derived parameters from these basic ones. In particular we define $\omega_c = \Delta b$. It follows that the power spectrum of V can be written $\tilde{C}(\omega) = 2\pi\delta x^2$ within the energy window ω_c and zero outside. Furthermore, we can define $\tau_{\text{cl}} = 1/\omega_c$ which is the classical correlation time of the power spectrum.

We present here a review of Kottos and Cohen, *et al.* [16] that studies the wave-packet dynamics in energy space of this model. This is the first step to understanding the more general and demanding problem of quantum dissipations in chaotic quantum systems. In order to study the wave-packet dynamics in energy space, we will introduce several measures that quantify the departure from the initial state. The three measure we will consider are:

1. The square root of the second moment of the energy distribution, defined to be

$$\delta E_{\text{tails}}(t) = \sqrt{\sum_i (E_i - E_\lambda)^2 P_t(i|\lambda)} \tag{4.33}$$

   This heavily weights the behavior far away from the state $|\lambda\rangle$ (the tails).

2. The δE_{core}, defined to be the energy range containing 50% of the evolving probability starting with the prepared site. That is to say, $\delta E_{\text{core}}(t)$ is defined to be the satisfy:

$$\frac{1}{2} \approx \sum_{k=-\delta E_{\text{core}}(t)/\Delta}^{\delta E_{\text{core}}(t)/\Delta} P(k|\lambda)(t).$$

   This quantity is very sensitive to the sites immediately surrounding the prepared state.

3. The survival probability, $P(t)$ defined to be,

$$P(t) = |\langle\lambda|\lambda(t)\rangle|^2 \tag{4.34}$$

where $|\lambda(t)\rangle$ is the time evolution of the prepared site $|\lambda\rangle$. This we have shown previously to be the time domain representation of the LDoS.

We begin the review with an analysis of the LDoS. It will be simpler to refer to the kernel, which we denote $P(i|\lambda) = |\langle i|\lambda\rangle|^2$ This analysis of the dynamical scenarios arising from this model is due to Cohen, *et al.*[9] and Hiller, *et al.* [16].

The following conventions will be used throughout this description:

- The standard perturbative regime occurs when $(\delta x/\Delta) \ll 1$.
- The extended perturbative regime occurs when $1 \ll (\delta x/\Delta) \ll b^{1/2}$
- The ergodic regime occurs when $b^{1/2} \ll (\delta x/\Delta) \ll b^{3/2}$

4.2.1 Parametric Evolution of the LDoS

We will see how the LDoS behaves as we transition from small δx to larger δx. In the standard perturbative regime, first order perturbation applies, and we get the usual result that,

$$P_{\mathrm{FOPT}}(n|\lambda) = \frac{\delta x^2 |V_{n\lambda}|^2}{(E_n - E_\lambda)^2} \tag{4.35}$$

for $n \neq \lambda$, and also $P_{\mathrm{FOPT}}(\lambda|\lambda) \approx 1$.

As δx increases, we enter the extended perturbative regime. In this regime, the LDoS within the bandwidth $(-\omega_c, \omega_c)$ takes on the same shape as in the Friedrich

model, namely a Lorentzian

$$P_{\text{prt}}(n|\lambda) = \frac{\delta x^2 |V_{n\lambda}|^2}{(E_n - E_\lambda)^2 + \Gamma^2} \tag{4.36}$$

of width $\Gamma = 2\pi(\delta x)^2/\Delta$. Outside the bandwidth, the LDoS decays faster than exponential. For stronger perturbations, the coupling is enough to causing strong mixing outside the bandwidth, which produces different dynamics.

Finally, when δx increases beyond perturbative results, the LDoS is described by a semicircle.

$$P_{\text{sc}}(n|\lambda) = \frac{1}{2\pi\Delta}\sqrt{4 - \left(\frac{E_n - E_\lambda}{\Delta}\right)^2}. \tag{4.37}$$

These three LDoS shapes are shown in Figure 4.5. The localization regime is also depicted, although it will not be considered in this text. This regime corresponds to perturbation strengths that are so large that $\mathcal{H}_0$ is considered a perturbation of V, rather than the other way around.

4.2.2 Wave-packet Dynamics

The wave-packet dynamics of the model under consideration does not have a straightforward description of the regimes as was found in the LDoS analysis of the last section. The main issue is whether or not Linear Response Theory (LRT) is applicable. For our purposes, we will consider a calculation within the domain of LRT if it depends only on the autocorrelation function $C(\tau)$ (this is the same as depending only on the band-profile of the perturbation operator). Now we will

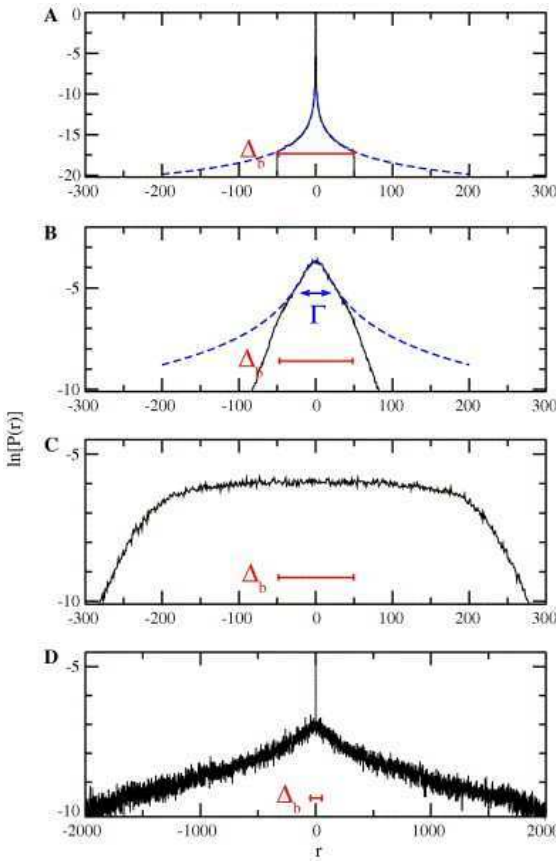

Figure 4.5: Simulations showing the shapes of the LDoS kernels in the various regimes. (a) standard perturbative (b) extended perturbative (c) ergodic (d) localization (not discussed here). Reproduced from [16].

consider time dependent driving. That is to say that $\mathcal{H} = \mathcal{H}_0 + \delta x(t)V$, where $\delta x(t) = \epsilon f(t)$ with ϵ controlling the strength of the driving. The LRT results are as follows:

The square root of the second moment is given by,

$$\delta E_{\text{tails}}(t) = \epsilon \times \sqrt{\int_{-\infty}^{\infty} \tilde{C}(\omega)\tilde{F}_t(\omega)\frac{d\omega}{2\pi}} \tag{4.38}$$

and the survival probability is given by,

$$P(t) = \exp\left(-\epsilon^2 \int_{-\infty}^{\infty} \tilde{C}(\omega)\frac{\tilde{F}_t(\omega)}{(\hbar\omega)^2}\frac{d\omega}{2\pi}\right) \tag{4.39}$$

where $\tilde{C}(\omega)$ is the usual power spectrum, and $\tilde{F}_t(\omega)$ is the spectral content of the driving $x(t)$, which is defined to be,

$$\tilde{F}_t(\omega) = \left|\int_0^t \dot{f}(t')e^{-i\omega t'}dt'\right|^2. \tag{4.40}$$

See Cohen and Kottos [13] for more on LRT. Now we will characterize the regimes for the wave-packet dynamics.

In the First Order Perturbation Theory Regime, the wave-packet dynamics are very simple. The prepared state is effectively only coupled to close by states. Therefore, both measures of the spreading of energy, will be on the order of the mean level spacing Δ, and the survival probability will be approximately unity.

In the extended perturbative regime, a core-tail structure develops, related to a separation of energy scales $\Delta \ll \delta E_{\text{core}}(t) \ll \delta E_{\text{tails}}(t) \sim \omega_c$. The core is non-

perturbative, but $\delta E_{\text{tails}}(t)$ is still determined by the perturbative tails.

In the non-perturbative region there is only one energy scale ω_c, and $\omega_c \ll \delta E_{\text{core}}(t) \sim \delta E_{\text{tails}}(t)$, and perturbation theory cannot be applied. Cohen, Izrailev, and Kottos [9] have proven that the spreading develops a diffusive component due to a random walk process of step $\hbar\omega_c$, which take place in the energy space. After this non-perturbative diffusive scale the packet again saturates occupying ergodically the energy shell. This ergodic behavior is shown in Figure 4.6 for an Effective Banded Random Matrix Model (EBRM), which is very similar to the Wigner BRM setup considered here [9].

4.3 Conclusion

In this section, we explored the emergence of the Fermi Golden Rule exponential decay. We calculated the LDoS of the flat Friedrichs model using algebraic means. From there, we investigated the effect of discreteness and level statistics. What we found was that the the level statistics of the discrete energies of the unperturbed Hamiltonian determined the shape of the revivals in the survival probability. Following this presentation, we then went on to review the literature on a setup closely related to the Friedrichs model, namely the Wigner Banded Random Matrix (WBRM) model. We distinguished between several regimes of the LDoS, which emerged by varying the perturbation strength, and we similarly saw the emergence of various regimes in the framework of the wave-packet dynamics. This review of the standard treatment of the subject of wave-packet dynamics in energy space of banded random matrices is the foundation for the next chapter,

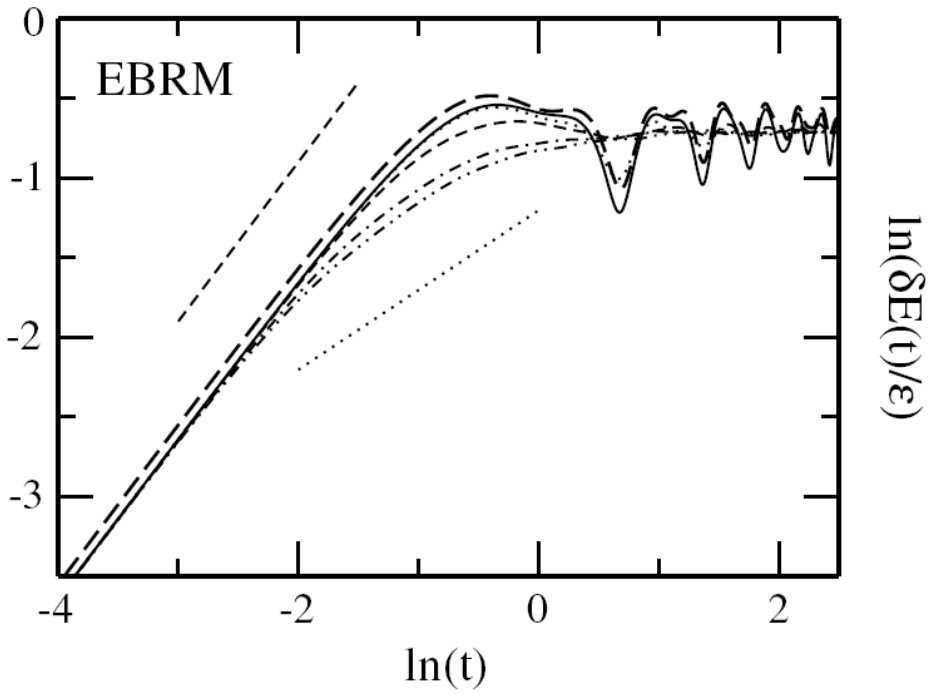

Figure 4.6: The quantity δE_{tails} for the EBRM model. The thick dashed line is the classical quantity, and the others are quantized results with various perturbation strengths. The gradual approach to saturation exhibited by the quantized model is indicative of the diffusive behavior. Reproduced from [16].

where we will consider a modification to the discussed setup that will result in fundamentally different dynamics.

5 Wave-Packet Dynamics of the Non-Flat Continuum

In the previous chapter, we discussed the wave-packet dynamics in energy space of complex systems described by a traditional Wigner Banded Matrix Model. The perturbation operator was characterized by some flat band-profile (with a finite cutoff in the case of Wigner model). Such RMT models describe chaotic systems with a classical power spectrum of the form $\tilde{C}(\omega) = 2\pi\epsilon^2$. However, in realistic circumstances one usually encounters situations where the perturbation operator has additional structure, like in the examples discussed in Chapter 2. This chapter deals with such a situation, i.e., wave-packet dynamics of systems with structured band-profiles. The results reported here are an extended version of the ones presented in our recent contribution [17], and to our knowledge constitutes the first theoretical investigation of the dynamical behavior of a RMT modeling with a non-trivial band-profile structure. In particular, we consider the dynamics generated by RMT models with the following power spectrum:

$$\tilde{C}(\omega) = \epsilon^2 |\omega|^{s-1}. \tag{5.1}$$

Our motivation for such a choice of the power spectrum is inspired by [33], where they have investigated the perturbation operator of a particle in a chaotic box under special families of perturbations: deformations and dilations of the box. The geometry and power spectrum are shown in Figure 5.1, and it is clear that the power-law behavior could described by Equation (5.1).

The most physically relevant model is the one where the prepared state is like all other states in the sea of levels (WM). But like before, this problem is not easily solved. This motivates us to consider simplified systems that will hopefully capture the relevant features of the WM. Therefore, we analyze first the FM, and derive a closed form expression for the survival probability. The decay is like $P(t) \sim (t/t_0)^{2s-4}$ for some t_0, where t_0 defines an important universal time scale of the problem. The functional form of the decay contrasts sharply with the flat scenario, which exhibits Fermi Golden Rule exponential decay.

We then will attempt to use the analysis of the FM to make predictions about the more physically meaningful WM, in which every level is itself coupled to the continuum by $\tilde{C}(\omega)$. To our surprise, we witness a first WBRM example for which the survival probability $P(t)$ behaves in a way that is not similar to the associated FM. Specifically we find that $P(t)$ is characterized by a generalized Wigner decay time t_0 that depends in a non-linear way on the strength of the coupling. We also establish that the scaled $P(t)$ has distinct universal and non-universal features. We conclude that it is only for the flat continuum that we get a robust exponential decay that is insensitive to the nature of the intra-continuum couplings. In addition to $P(t)$ we will also investigate other measures of the

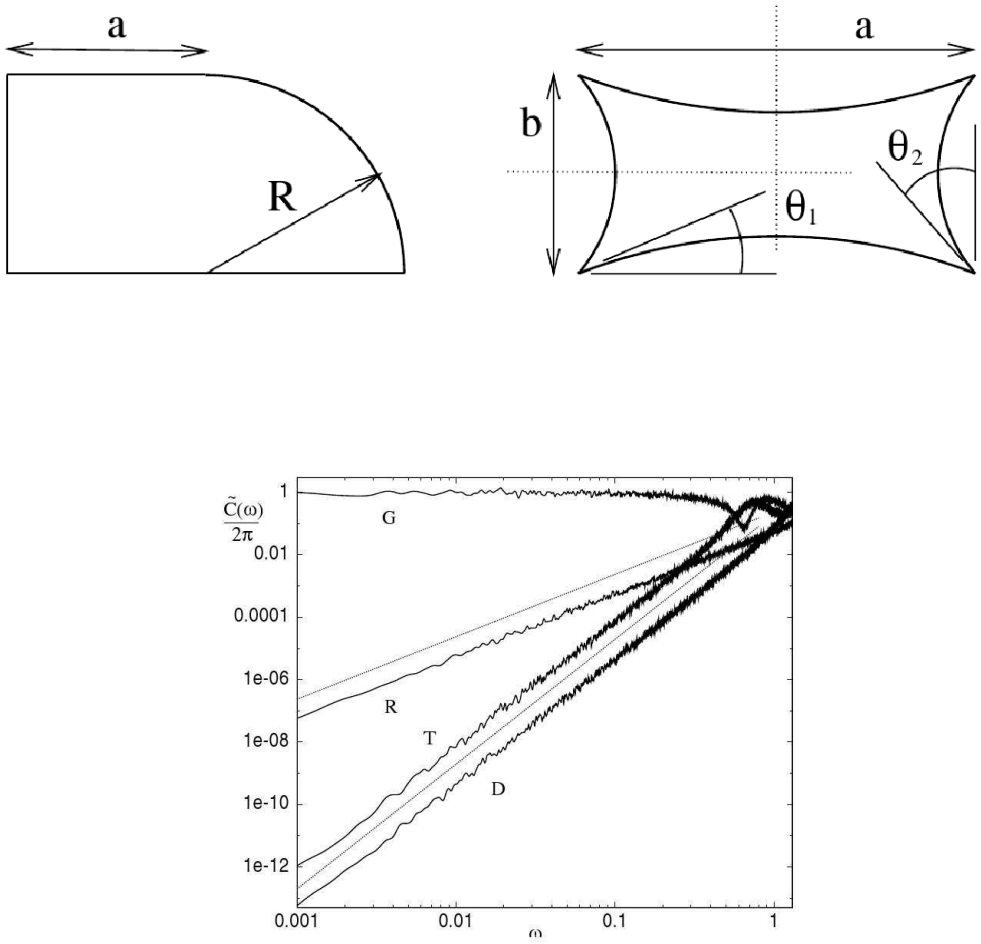

Figure 5.1: *(top)* The billiards whose geometry will be deformed. *(bottom)* The power spectrum of the fluctuations for various types of deformations. Notice that most of the deformations have a power law as in Equation (5.1) Reproduced from [33]

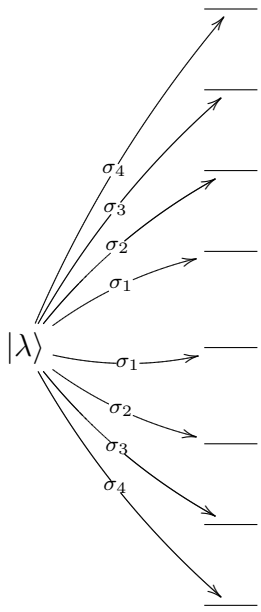

Figure 5.2: Graph theoretic representation of the Friedrichs model. Each σ_k represents the variance of the coupling of $|\lambda\rangle$ to a location in the continuum. $\sigma_k = \epsilon^2(k\Delta)^{s-1}$ where Δ is the level spacing.

spreading like the second moment of the evolving wave-packet. Our theoretical results will be always contrasted with detailed numerical calculations.

5.1 Decay of a Bound State to a Non-Flat Continuum

Let $\mathcal{H} = \mathcal{H}_0 + V$ be a Hamiltonian where $\mathcal{H}_0$ is the Hamiltonian of the unperturbed system having a picket fence spectrum with mean level spacing Δ, while V describes the perturbation. Let $|\lambda\rangle$ be an eigenstate of $\mathcal{H}_0$ in the middle of the energy spectrum, and assume that the system is prepared in state $|\lambda\rangle$ at time

$$\begin{pmatrix}
E_1 & 0 & \cdots & 0 & \sigma_1 & 0 & 0 & \cdots & 0 \\
0 & E_2 & \cdots & 0 & \sigma_2 & 0 & 0 & \cdots & 0 \\
0 & 0 & \ddots & \vdots & \vdots & \vdots & \vdots & \ddots & \vdots \\
\vdots & \vdots & & E_{\lambda-1} & \sigma_{\lambda-1} & 0 & 0 & 0 & 0 \\
\sigma_1 & \sigma_2 & \cdots & \sigma_{\lambda-1} & E_\lambda & \sigma_{\lambda+1} & \sigma_{\lambda+2} & \cdots & \sigma_N \\
0 & 0 & \vdots & 0 & \sigma_{\lambda+1} & E_{\lambda+1} & 0 & \cdots & 0 \\
0 & 0 & \vdots & 0 & \sigma_{\lambda+2} & 0 & E_{\lambda+2} & & \vdots \\
\vdots & \vdots & \ddots & \vdots & \vdots & \vdots & \vdots & \ddots & 0 \\
0 & 0 & \cdots & 0 & \sigma_N & 0 & 0 & \cdots & E_N
\end{pmatrix}$$

Figure 5.3: Matrix representation of the total Hamiltonian $\mathcal{H}$ written in the basis of $\mathcal{H}_0$.

$t = 0$. This state subsequently decays to a sea of other states due to the coupling of V. The perturbation matrix V is determined by Equation (2.4) and the spectral density function:

$$\tilde{C}_\lambda(\omega) = \begin{cases} \epsilon^2 |\omega|^{s-1} & |\omega| \leq \omega_c \\ 0 & |\omega| > \omega_c \end{cases} \tag{5.2}$$

The subscript λ in the above expression indicates the fact that only the distinguished energy level E_λ is coupled to the rest of the levels by the rank two matrix V. A visualization of the perturbation matrix is shown in Figure 5.3. A graph theoretic representation of the total Hamiltonian is given in Figure 5.2.

Occasionally it will be useful to think of the "smooth" power spectrum,

$$\tilde{C}(\omega) = \epsilon^2 |\omega|^{s-1} e^{-|\omega|/\omega_c} \tag{5.3}$$

for all ω. This smooth expression introduces the cutoff, ω_c, through an exponential in order to simplify the calculus involved in certain Fourier transforms. This is not such a dramatic change to the problem, and we will provide numerical evidence to suggest that this change does not alter the results significantly.

Notice that when $s = 1$, the problem reduces to the flat case considered in Chapter 4. Furthermore, for $s > 2$, the model can be treated by using first order perturbation theory. The theory we will develop in this chapter only applies for $1 \leq s \leq 2$. The situation where $s < 1$ would require a more complex treatment because of the increased importance of level statistics. The model is completely determined by the parameters $(s, \epsilon, \Delta, \omega_c)$.

It is evident from the dimensional analysis that there are three relevant time scales: The Heisenberg time t_H, which is related to the mean level spacing Δ, the semi-classical (correlation) time, which is related to the bandwidth ω_c, and the generalized Wigner decay time t_0, which is related to the strength of the driving. Summarizing these time scales we have:

- $t_{\mathrm{H}} = 1/\Delta$
- $\tau_{\mathrm{cl}} = 2\pi/\omega_c$
- $t_0 = \left(\frac{|\sin s\pi/2|}{\pi\epsilon^2}\right)^{\frac{1}{2-s}}$

The significance of t_0 will be justified in the next section. It is related to a characteristic energy that defines a crossover from one behavior to another in the LDoS. The Heisenberg time determines the onset to quantum recurrences. In the continuum limit, this time tends towards infinity. Similarly, as the limit of the

bandwidth tends towards infinity, $\tau_{\rm cl}$ tends towards zero. Thus in these limits, the only time scale that remains is t_0.

We will now determine the boundaries for ϵ given a fixed (s, Δ, ω_c). This will be especially important for the numerical simulations. The theory must take place in a time window before the Heisenberg time, in order to avoid recurrences, and after $\tau_{\rm cl}$ in order to be non-perturbative. Thus, we have the restriction $\tau_{\rm cl} \ll t_0 \ll t_{\rm H}$. In other words,

$$\frac{1}{\omega_c} \ll t_0 \ll \frac{1}{\Delta}. \tag{5.4}$$

Direct substitution yields the bounds on ϵ, which are:

$$(\Delta|\sin s\pi/2|)^{\frac{2-s}{2}} \ll \epsilon \ll \left(\Delta\frac{N}{2}|\sin s\pi/2|\right)^{\frac{2-s}{2}}. \tag{5.5}$$

All numerics discussed regarding this model occur in the regime defined by Equation (5.5).

5.1.1 The Local Density of States

Following the same strategy as in Chapter 4, we calculate the LDoS associated with the non-flat FM. Its Fourier transform will give us the survival probability amplitude. Our approach to the LDoS will differ from the one of the previous chapter, where attention was paid also to the spectral properties of the unperturbed Hamiltonian. Specifically, in this derivation we will use the so-called Feshbach projection method. The main idea is to decompose the Hilbert space into two

subspaces $\mathcal{P}$ and $\mathcal{Q}$. The subspace $\mathcal{P}$ only contains the prepared state $|\lambda\rangle$, while $\mathcal{Q}$ is associated with the continuum. The Hamiltonian $\mathcal{H}$ projected into the $\mathcal{P}$ subspace will be the effective Hamiltonian for the state $|\lambda\rangle$, since it will generate the dynamics of $|\lambda\rangle$. Then one can calculate $\langle\lambda| G^+ |\lambda\rangle$, where G^+ is the retarded Green's function for the effective Hamiltonian. This overlap element is directly related to the LDoS (see Appendix B.1). Referring to the Appendix B.2 for a detailed derivation, we get that the LDoS for the non-flat FM is

$$\rho(\omega) = \frac{1}{\pi} \frac{\Gamma(\omega)/2}{(\omega - \Delta(\omega))^2 + \Gamma(\omega)/2)^2}, \tag{5.6}$$

which resembles a Lorentzian. The functions $\Gamma(\omega)$, $\Delta(\omega)$ are defined to be,

$$\begin{aligned} \Delta(\omega) &= \sum_{n \neq 0} \frac{|V_{n,0}|^2}{E_0 - E_n} = \int_{-\infty}^{\infty} \frac{\tilde{C}(\omega')}{\omega - \omega'} d\omega' \\ \Gamma(\omega) &= 2\pi \sum_n |V_{0,n}|^2 \delta(\omega - E_n) \equiv 2\pi \tilde{C}(\omega) \end{aligned} \tag{5.7}$$

and in Appendix B.3 we show that these evaluate to,

$$\begin{aligned} \Delta(\omega) &= \epsilon^2 \pi \omega |\omega|^{s-2} \cot \frac{s\pi}{2} \\ \Gamma(\omega) &= 2\pi\epsilon^2 |\omega|^{s-1}. \end{aligned} \tag{5.8}$$

Simple algebraic substitution reveals that the LDoS of this problem is:

$$\rho(\omega) = \frac{\epsilon^2}{|\omega|^{3-s} - (2\pi\epsilon^2 \cot \frac{s\pi}{2})|\omega| + (\pi^2\epsilon^4 / \sin^2 \frac{s\pi}{2})|\omega|^{s-1}} \tag{5.9}$$

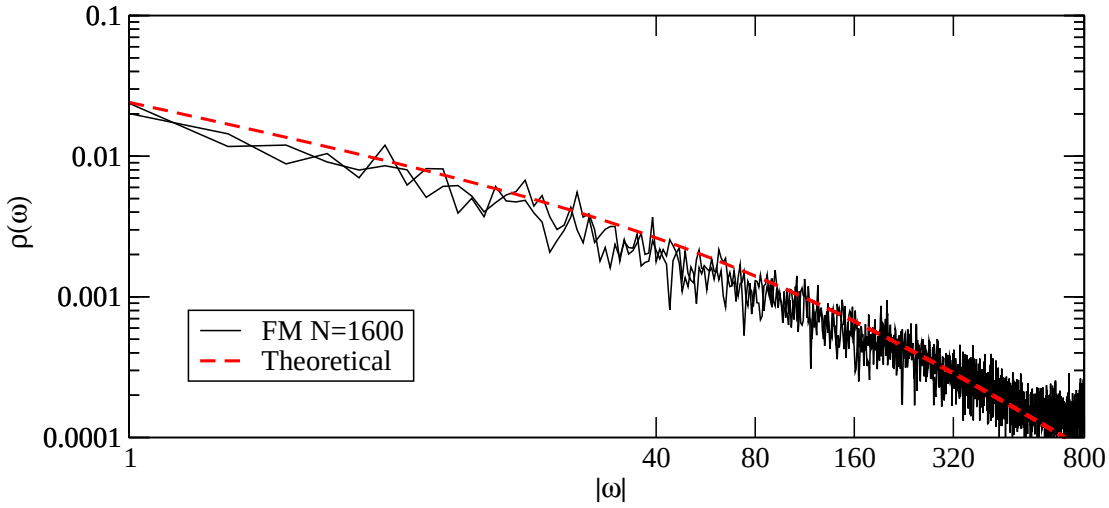

Figure 5.4: LDoS of the Friedrichs model. In this case $s = 1.5$ and $\epsilon = 1.44$. The theoretical line is Equation (5.9). The numerics were performed by diagonalization of 100 realizations of the Hamiltonian.

In order to gain some confidence in our analytical calculations, we have also evaluated the LDoS for the FM numerically. The results of our numerical investigations are reported along with this theoretical LDoS in Figure 5.4. We observe an excellent agreement between the analytics and the numerics.

The next step is to identify the regions defined by the dominant terms of the denominator. We argue that the linear term is never dominant. Indeed, if we write the denominator as,

$$|\omega|^{3-s} - (2\pi\epsilon^2 \cot\frac{s\pi}{2})|\omega| + (\pi^2\epsilon^4/\sin^2\frac{s\pi}{2})|\omega|^{s-1} = 2\pi\epsilon^2 \cot\frac{s\pi}{2}|\omega| \left[\frac{|\omega|^{2-s}}{2\pi\epsilon^2 \cot s\pi/2} + \frac{\pi^2\epsilon^4|\omega|^{s-2}}{2\pi\epsilon^2 \cot\frac{s\pi}{2}\sin^2\frac{s\pi}{2}} - 1\right]. \tag{5.10}$$

the linear term is dominant when the quantity in brackets is approximately -1,

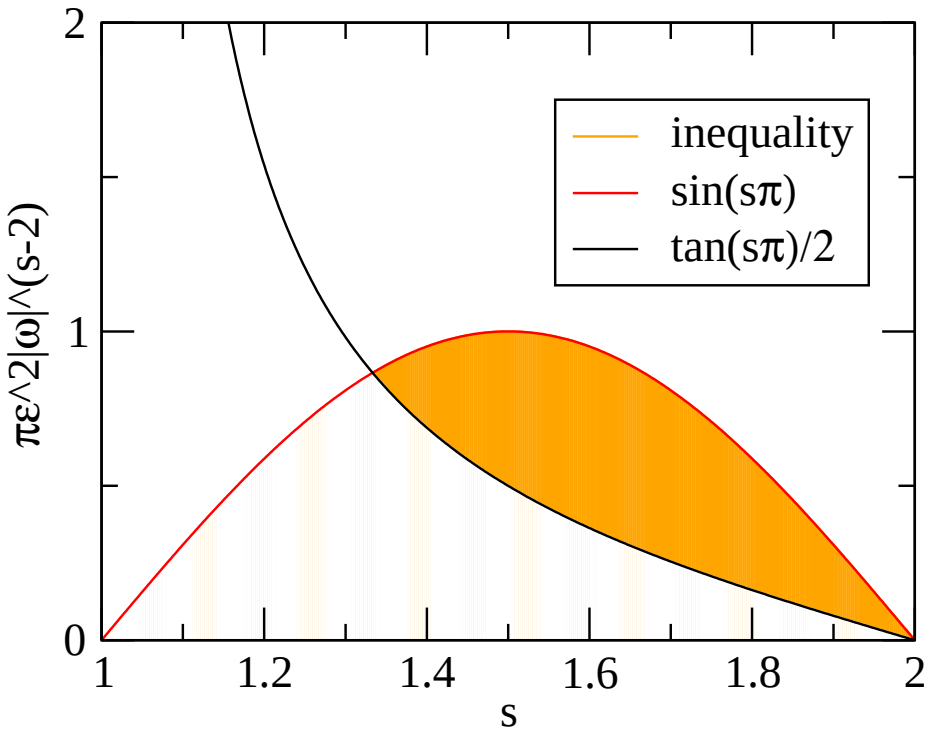

Figure 5.5: Plot of the inequality (5.11) where the y axis is $\pi\epsilon^2|\omega|^{s-2}$

which means that

$$\left|\frac{\tan\frac{s\pi}{2}}{2\pi\epsilon^2}\right| \ll |\omega|^{s-2} \ll \left|\frac{\sin s\pi}{\pi\epsilon^2}\right| \tag{5.11}$$

This inequality is satisfied in the shaded region in Figure 5.5. Observe in this figure that for any s, the inequality is satisfied for less than an order of magnitude, so in order to see an ω window where the linear term dominates, it is necessary to make ϵ^2 small, but when this happens, we are back to simple perturbative calculations. Thus we can conclude that the linear term of the denominator never dominates.

It remains to compare $(\pi^2\epsilon^4/\sin^2\frac{s\pi}{2})|\omega|^{s-1}$ with $|\omega|^{3-s}$. We write,

$$|\omega|^{3-s}+(\pi^2\epsilon^4/\sin^2\frac{s\pi}{2})|\omega|^{s-1}=|\omega|^{s-1}\frac{\pi^2\epsilon^4}{\sin^2\frac{s\pi}{2}}\left[\left(\frac{|\omega|^{2-s}}{\left(\frac{\pi\epsilon^2}{\sin\frac{s\pi}{2}}\right)}\right)^2+1\right]. \tag{5.12}$$

Which apparently means that when $|\omega|^{2-s}\ll\frac{\pi\epsilon^2}{|\sin\frac{s\pi}{2}|}$, the $|\omega|^{s-1}$ term dominates. Similarly, we can write,

$$|\omega|^{3-s}+(\pi^2\epsilon^4/\sin^2\frac{s\pi}{2})|\omega|^{s-1}=|\omega|^{3-s}\left[1+\left(\frac{\left(\frac{\pi\epsilon^2}{\sin s\pi/2}\right)}{|\omega|^{2-s}}\right)^2\right] \tag{5.13}$$

This allows us to conclude that when $|\omega|^{2-s}\gg\frac{\pi\epsilon^2}{|\sin\frac{s\pi}{2}|}$, the $|\omega|^{3-s}$ term dominates.

Summarizing the above approximations for the LDoS, we have:

$$\rho(\omega)=\begin{cases}\frac{\sin^2 s\pi/2}{\pi^2\epsilon^2}\frac{1}{|\omega|^{s-1}} & |\omega|^{2-s}\ll\frac{\pi\epsilon^2}{|\sin s\pi/2|}\\ \frac{\epsilon^2}{|\omega|^{3-s}} & |\omega|^{2-s}\gg\frac{\pi\epsilon^2}{|\sin s\pi/2|}\end{cases} \tag{5.14}$$

Furthermore, the energy level,

$$\omega_0=\left(\frac{\pi\epsilon^2}{|\sin s\pi/2|}\right)^{\frac{1}{2-s}} \tag{5.15}$$

and the corresponding time,

$$t_0=\left(\frac{|\sin s\pi/2|}{\pi\epsilon^2}\right)^{\frac{1}{2-s}} \tag{5.16}$$

emerge as fundamental quantities of the LDoS analysis.

5.1.2 Survival Probability

The LDoS of the FM is neatly split into a low energy and high energy region with crossover at $1/t_0$. Therefore, we can reasonably expect that the Fourier transform of each region in energy space as if it were extended over all energies will agree with the survival probability amplitude in the corresponding region. The low energy region of the LDoS determines the long time behavior of the survival probability amplitude, and the high energy region of the LDoS determines the short time behavior.

Taking the limit $\omega_c \to \infty$, we evaluate the Fourier transforms of the limiting expressions for the LDoS as in Equation (5.14). We find that the survival probability amplitude is $1-(t/t_0)^{2-s}$ for short times and $1/(t/t_0)^{2-s}$ for long times with crossover at t_0. Therefore the survival probability is given by,

$$P(t) = \begin{cases} 1-(t/t_0)^{4-2s} & t \ll t_0 \\ (t/t_0)^{2s-4} & t \gg t_0 \end{cases} \tag{5.17}$$

Unfortunately, in our numerical investigation of the survival probability, it has not been possible to observe the $t \ll t_0$ power law due to the initial Gaussian decay dominating the short time behavior. The $t \gg t_0$ power-law, however, is robust, and is confirmed in Figure 5.6. This data was generated by the numerical integration of the Shrödinger equation using the same algorithm as in the flat continuum simulations.

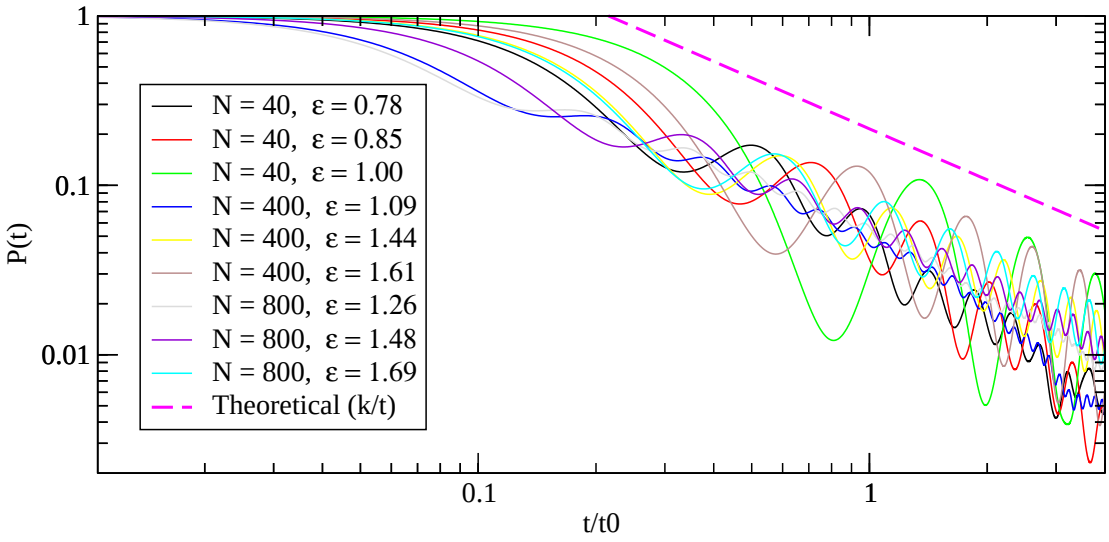

Figure 5.6: Survival probability, with t_0 time scaling

5.1.3 Other Measure of Energy Spreading

We return to the two measures of energy spreading discussed in Chapter 4: $\delta E_{\text{core}}(t)$ and $\delta E_{\text{tails}}(t)$. As indicated by their subscripts, each quantity weights more heavily either the spreading in the core or the spreading at the tails more heavily than the other. Furthermore, in this section we will see that these measures have different time and energy scales, indicating that the physics of the core is different from the physics of the tails.

In Appendix C, we deduce the time and energy scales of systems described systems characterized by the power spectrum as in Equation (2.4). The conclusion of the argument is that the time scaling is $t \mapsto \sqrt{\frac{s}{s+2}}\omega_c t$, and the energy scaling is by $\delta E_{\text{tails}}(t)$ is $\delta E_{\text{tails}}(t) \mapsto \sqrt{\frac{s}{\epsilon^2 \omega_c^s}}\delta E_{\text{tails}}(t)$. In Figure 5.7, we present the scaled $\delta E_{\text{tails}}(t)$ for various parameters, and we observe that, indeed, the scaling law is

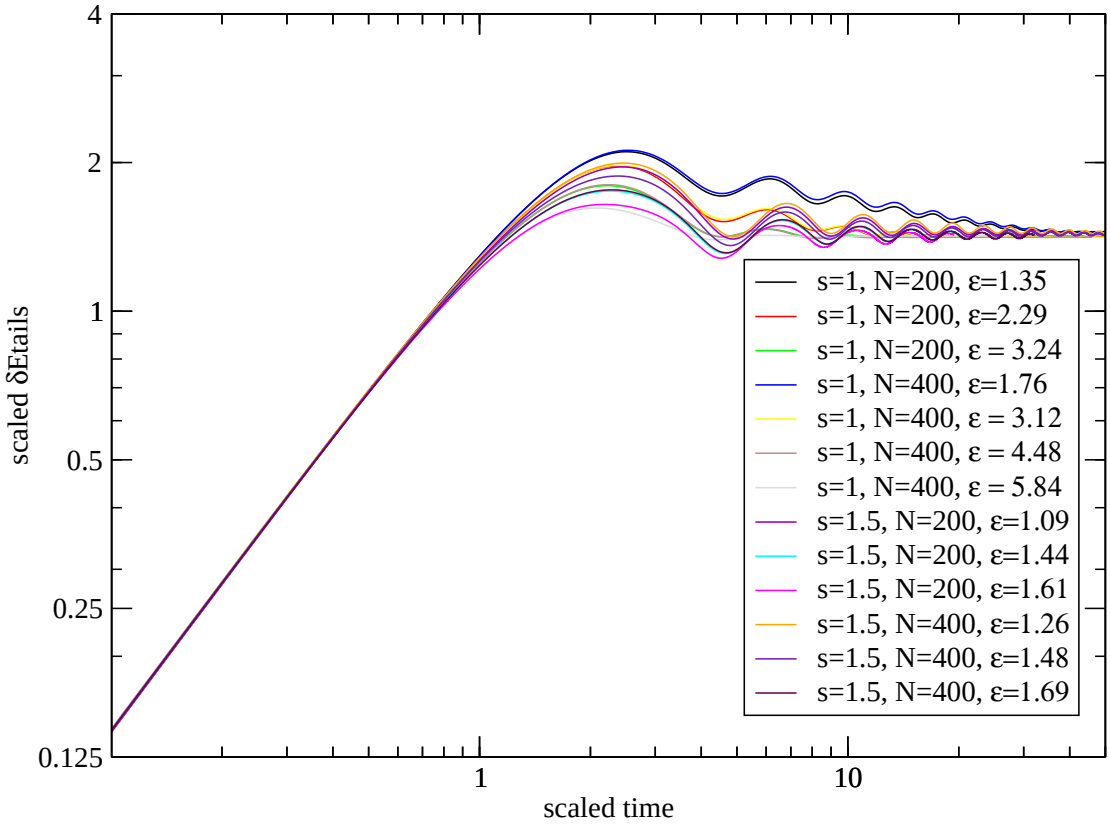

Figure 5.7: $\delta E_{\text{tails}}(t)$ with $\delta E_{\text{tails}}(t) \mapsto \sqrt{\frac{s}{\epsilon^2 \omega_c^s}} \delta E_{\text{tails}}(t)$, $t \mapsto \sqrt{\frac{s}{s+2}} \omega_c t$ scaling.

correct.

The quantity $\delta E_{\text{core}}(t)$ is closely related to the survival probability, so the time scaling of $\delta E_{\text{core}}(t)$ should go like t_0. Furthermore, the quantity the energy scale should also be related to t_0, namely its associated energy $1/t_0$. Thus, we reason that the appropriate scaling law for $\delta E_{\text{core}}(t)$ is $\delta E_{\text{core}}(t) \mapsto \delta E_{\text{core}}(t) * t_0$ and $t \mapsto t/t_0$. We plot $\delta E_{\text{core}}(t)$ for various parameter in Figure 5.8 with the scaling described above. This scaling is not especially good. In order to understand what is happening, we characterize each curve by a single value, called the **departure**

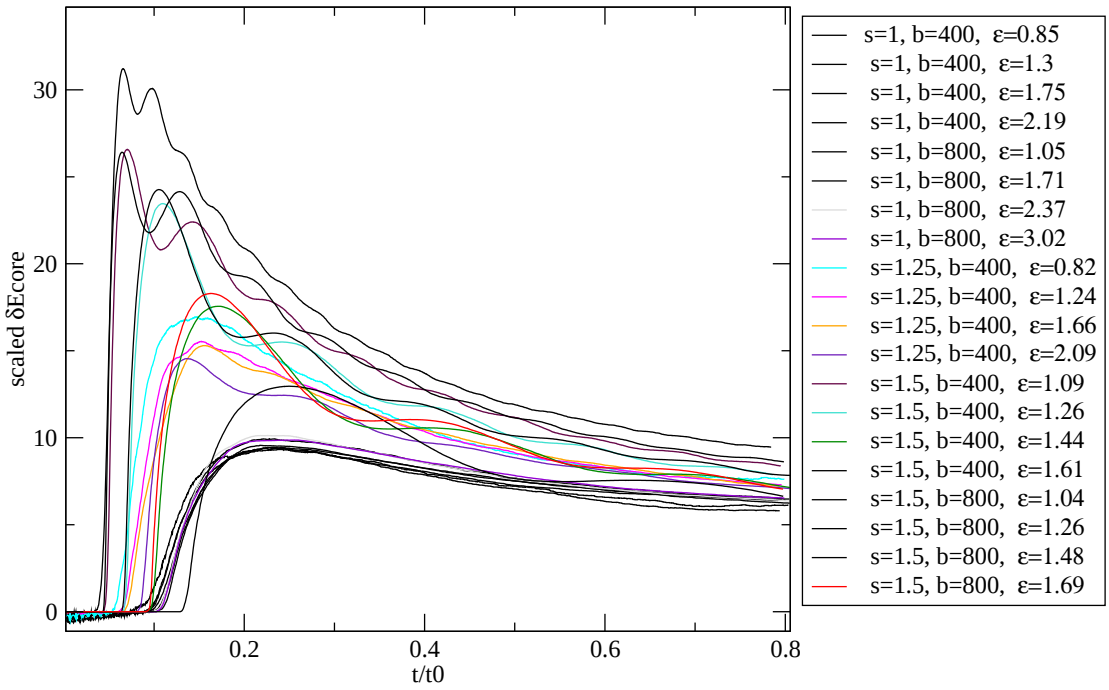

Figure 5.8: $\delta E_{\text{core}}(t)$ with $\delta E_{\text{core}}(t) \mapsto \delta E_{\text{core}}(t) * t_0$ and $t \mapsto t/t_0$ scaling.

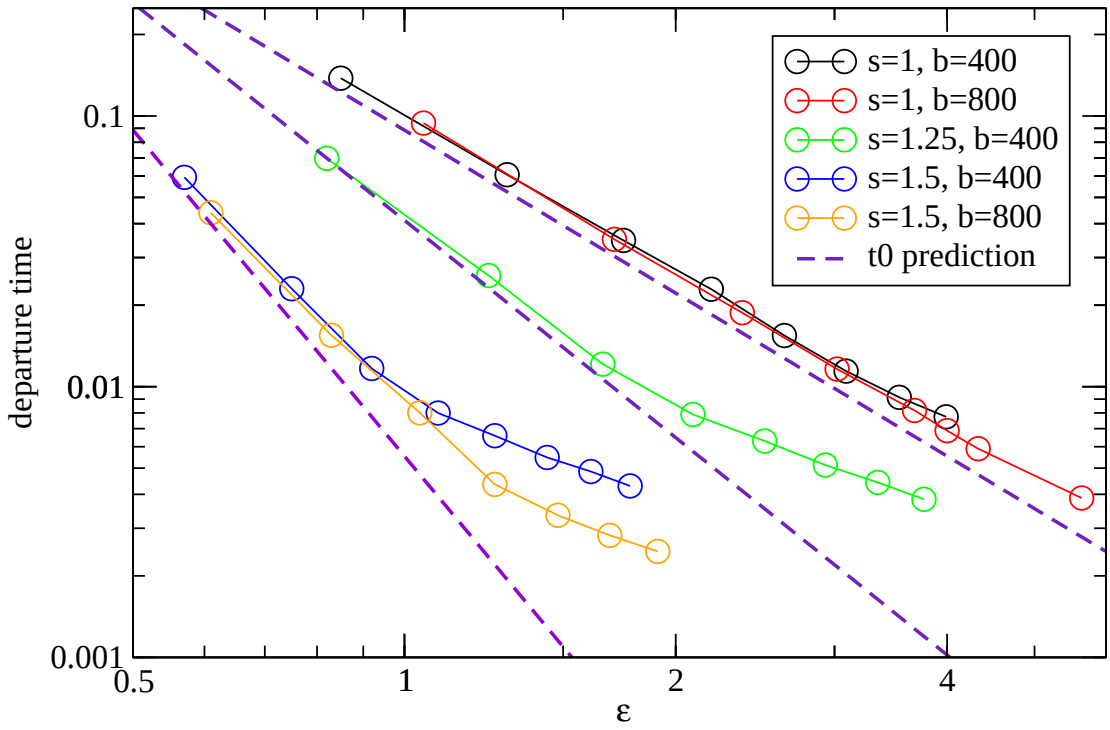

Figure 5.9: Extracted departure times vs. perturbation strength, ϵ. The dashed lines are the t_0 prediction.

point. The departure point is the first time that $\delta E_{\text{core}}(t)$ changes from unity. The departure points should vary like t_0. The departure points and the t_0 prediction are plotted in Figure 5.9. In this presentation, it becomes clear that the t_0 scaling is appropriate for small ϵ, but breaks down as ϵ increases. We will defer the discussion of this topic to its treatment in the Wigner Model, where we will be able to give a more satisfying explanation for these deviations.

5.2 The Wigner Model

In the last part of this Chapter we discuss the wave-packet dynamics in energy space for the Wigner Model (WM). In contrast to the FM discussed in the previous section, the perturbation V in the the WM is a banded matrix of width $\omega_c = \Delta b$ and it does not distinguishes between the levels. V is a random matrix whose band-profile is characterized by the power spectrum:

$$\tilde{C}(\omega) = \begin{cases} \epsilon^2 |\omega|^{s-1} & |\omega| \leq \omega_c \\ 0 & |\omega| > \omega_c \end{cases} \tag{5.18}$$

5.2.1 The Local Density of States

In Chapter 4, we saw that the Friedrichs model and the Wigner model had the same LDoS within the energy range $(-\omega_c, \omega_c)$. As a result, the survival probability in both cases decayed exponentially with the same scaling law. The justification for the similarity of the LDoS was minimal. We might expect that the same correspondence applies here as well, but the agreement between the models is limited. This indicates to us that *the nature of intra-continuum couplings significantly determines the relaxation process.* There is a fundamental difference between the LDoS in the Friedrich model for $s = 1$ and $s > 1$. Indeed, as we have shown previously, the LDoS for the Friedrichs model diverges at the origin for $s > 1$, while for $s = 1$, it does not. This is important, because the LDoS of the WM for $s > 1$ does not diverge at the origin.

The analysis of the LDoS in the WM case can be carried out approximately

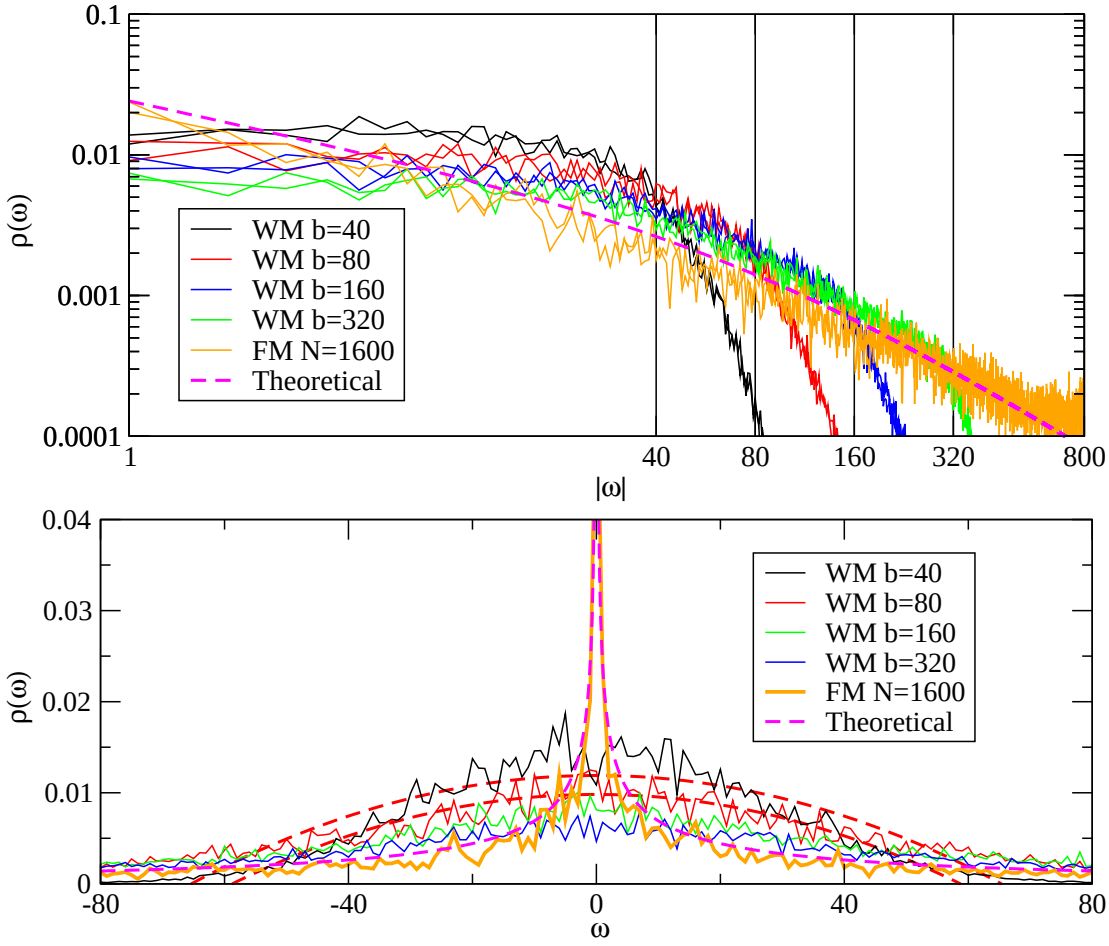

Figure 5.10: LDoS of the Wigner and Friedrichs models plotted log-log and log-linear. For all curves, $s = 1.5$ and $\epsilon = 1.44$. The theoretical line for the FM is Equation (5.9). (*top*) The LDoS of the FM and WM show agreement for the tails until the cutoff ω_c. (*bottom*) The core is fundamentally different for WM and FM. The theoretical lines for the WM are regressions of a semicircular function. Notice that the LDoS of the Friedrichs model diverges around $\omega = 0$, but this is not the case in the Wigner model.

using a blend of heuristic and formal methods. As already observed in previous works [9] (and see Figure 5.10) the LDoS has first order tails $|V_{n,\lambda}/(E_n - E_\lambda)|^2$ that coexist with the core (non-perturbative) component. We can determine the border γ_0 between the core and the tail simply from normalization:

$$p_0 = \int_{\gamma_0}^{\infty} \frac{\tilde{C}(\omega)}{\omega^2} d\omega \sim 1 \tag{5.19}$$

Some very preliminary results (see also next section) indicate that the resulting γ_0 is directly related to the t_0 of the FM. For $s > 2$ we would have for sufficiently small coupling $p_0 \ll 1$ even if we took the limit $\gamma_0 \to 0$. This means that first order perturbation theory is valid as a global approximation. But for $s < 2$, the above equation implies breakdown of first order perturbation theory at γ_0. In the tails $\mathcal{H}_0$ dominates over V, while in the core V dominates. Therefore, as far as the core in concerned, it makes sense to diagonalize V with an effective cutoff γ_0. Following the arguments of Feingold [34] concerning the diagonalization of random banded matrices, the result for the LDoS core shape should be semicircle-like, i.e.,

$$\rho(\omega) \approx 1 - (\omega/R)^2 \qquad \text{for } \omega/R << 1 \tag{5.20}$$

with width R given by the expression by

$$\Delta E_{\text{sc}} = \left[\int_0^{\gamma_0} \tilde{C}(\omega) d\omega \right]^{1/2} \sim \gamma_0 \tag{5.21}$$

We emphasize that in order to obtain the last equality we have to use the *effective*

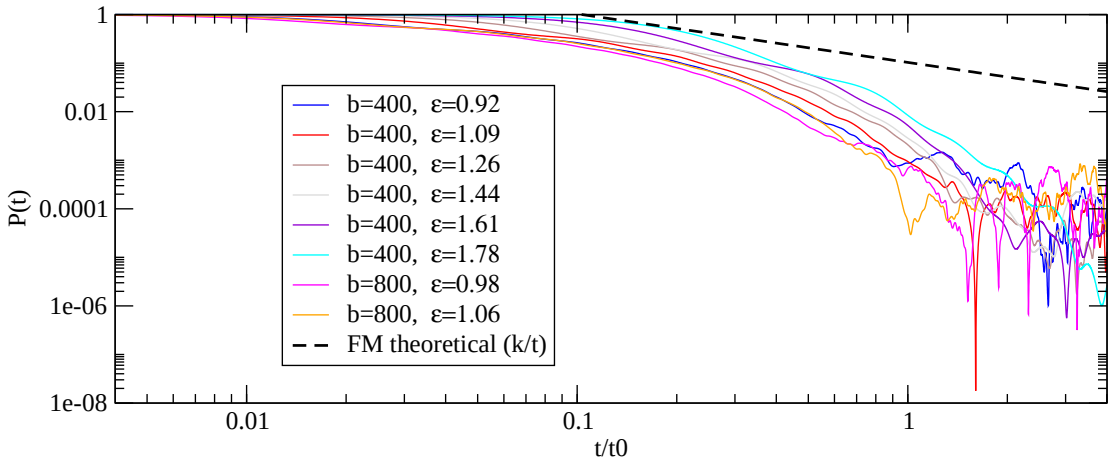

Figure 5.11: Survival probability for the non-flat Wigner Model. For all curves, $s = 1.5$. The scaling relation is from the FM, and the theoretical line is also from the FM.

bandwidth γ_0 instead of the actual bandwidth ω_c. The outcome demonstrates that our procedure is self-consistent: the core has the same width as implied by the breakdown of first-order perturbation theory. We note that within this perspective, the $s = 1$ Lorentzian is regarded as composed of a semicircle-like core and first order tails. The applicability of our analytical argumentation was tested via direct numerical evaluation of the LDoS for the Wigner model. In Figure 5.10, we report the outcome of our numerical results together with the theoretical expectations. One can clearly see two distinct regimes: the core, which can be described by a semicircle, and the tails, which are described by a similar expression as the one for the FM.

5.2.2 Survival Probability

Next we look at the survival probability of the Wigner model. We will assume that the energy scale that determines the change in the functional form of the LDoS is the relevant one that dictates the temporal behavior of the survival probability. Following this ansatz, we report in Figure 5.11 the survival probabilities of the WM with $s = 1.5$ for various bandwidths b and perturbation strengths ϵ. A moderately good scaling behavior is observed. Nevertheless, more work is needed in order to establish for certain that the relevant scaling time for the Wigner model is the same as the scaling time of the FM. Another fundamental point of our calculation is the drastic deviation of the decay law for the WM compared with the decay law for the relaxation process of the FM (see bold dashed line in Figure 5.11).

Naively we assume that the time scale behaves like in the FM. Figure 5.11 shows that there is limited agreement with the scaling, but an entirely different functional shape. This is to be expected, because the LDoS and survival probability are different representations of each other. Apparently in the WM case, there is some other characteristic time and energy that governs the dynamics. The t_0 scaling is not entirely wrong, but it is apparent that a more refined study of the LDoS is required.

5.2.3 Other Measures of Energy Spreading

In addition to the survival probability, we consider two other measures to characterize the spreading of energy from the prepared state to the continuum.

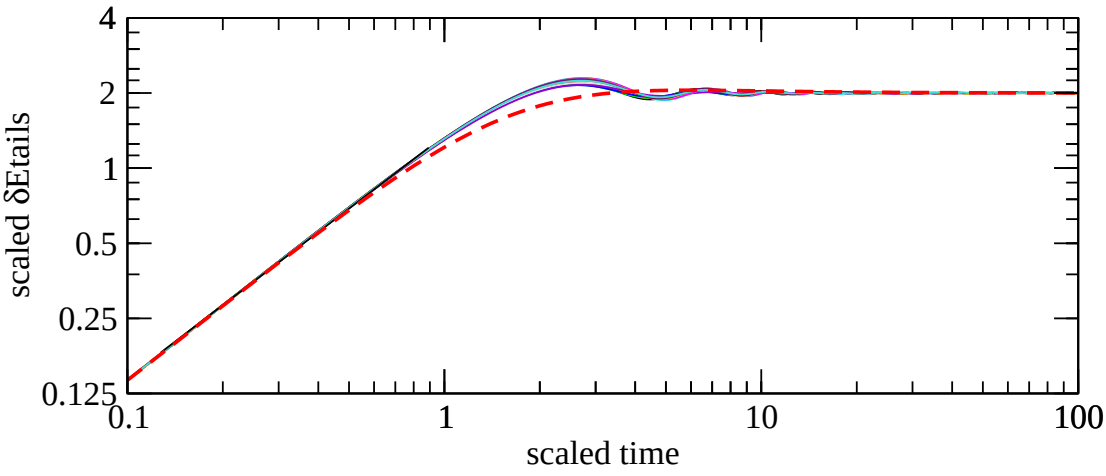

Figure 5.12: $\delta E_{\text{tails}}(t)$ for the WM. The dashed red line comes from numerical integration of the power spectrum. The other curves are representatives for the parameters $s = 1, 1.25$ and 1.5, $b = 400$ and 800, with various values of ϵ within the bounds discussed in Section (5.5).

The arguments regarding the scaling relations for the $\delta E_{\text{tails}}(t)$ is derived in Appendix C. This is the same argument that applied to the FM, which is appropriate because the power spectrums are the same in both cases, and the argument about δE_{tails} depends only on the power spectrum. The numerical results with the appropriate scaling are shown in Figure 5.12. One difference to note is that the steady state for the WM is a factor of $\sqrt{2}$ times higher than the FM case.

The δE_{core}

In the case of $s = 1$, we found that the standard deviation of the evolving energy distribution $\delta E_{\text{tails}}(t)$ and the core of the distribution $\delta E_{\text{core}}(t)$ scale in a different manner. We concluded that this reflects the different type of physics governing the core and the tail of the distribution. The former is dictated by γ_0 while the

latter is related to by ω_c. We carry out the same type of investigation for the $s > 1$ case.

In Figure 5.13 we report some representative cases of the $\delta E_{\rm core}$ versus time. We see that originally $\delta E_{\rm core} = 1$ (as always, we assume that the mean level spacing is $\Delta = 1$). As long as $\delta E_{\rm core} \approx \Delta$, most of the probability is concentrated in only one level (the initial state) and thus standard first order time-dependent perturbation theory is applicable to describe the evolving energy distribution. At a later time t^*, we observe a sudden departure towards a saturation value. The transition is quite sharp and one can extract easily the t^* from the numerical simulations. Its existence signifies the creation of a "core" area of the evolving profile. The sharp nature of the transition indicates that the core is formed very rapidly. This is the energy regime where the shape of the evolving energy distribution is highly non-perturbative. In Figure 5.14 we plot the extracted time t^* versus the inverse of the saturation plateau reached by $\delta E_{\rm core}$. We see that both of them are related in a linear way, thus indicating that the width of the core is inversely proportional to the departure time t^*. On the other hand, from the LDoS analysis we have that the LDoS core is related to the energy scale $\gamma_0 \sim 1/t_0$, where t_0 is the time scale for the Friedrichs model. It is therefore natural to investigate the possibility that $1/t^* \sim \delta E_{\rm core}^{\rm satur} \sim \gamma_0 \sim 1/t_0$. Indeed, in Figure 5.15 we report our numerical data for various values of s showing the departure time t^* vs. the perturbation strength ϵ. The bold dashed lines indicate the theoretical expectation for the case where t^* scales accordingly to the ansatz above (i.e. accordingly to t_0). A moderate agreement is evident. The deviations are attributed to a finite bandwidth effect.

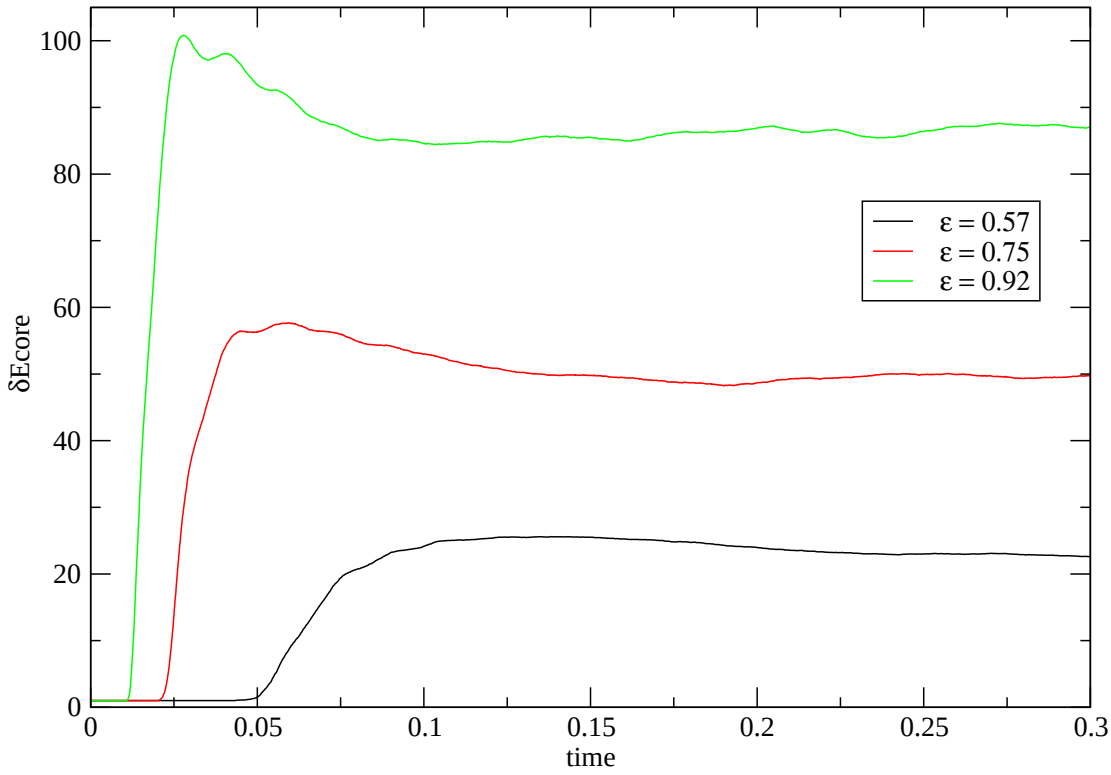

Figure 5.13: Unscaled δE_{core} vs. time for the WM. δE_{core} is strictly 1 up to some time t^*, after which it increases sharply until saturation.For all curves $s = 1.5$ and $b = 400$.

The justification for this claim is that in Figure 5.15, it is apparent that increasing the bandwidth b decreases the deviation from the predicted line.

5.3 Conclusion

In this chapter we analyzed two models with non-flat power spectrum: The Friedrichs model and the Wigner model. We found that first order tails of the LDoS are fully determined by the spectral density function $\tilde{C}(\omega)$, which also al-

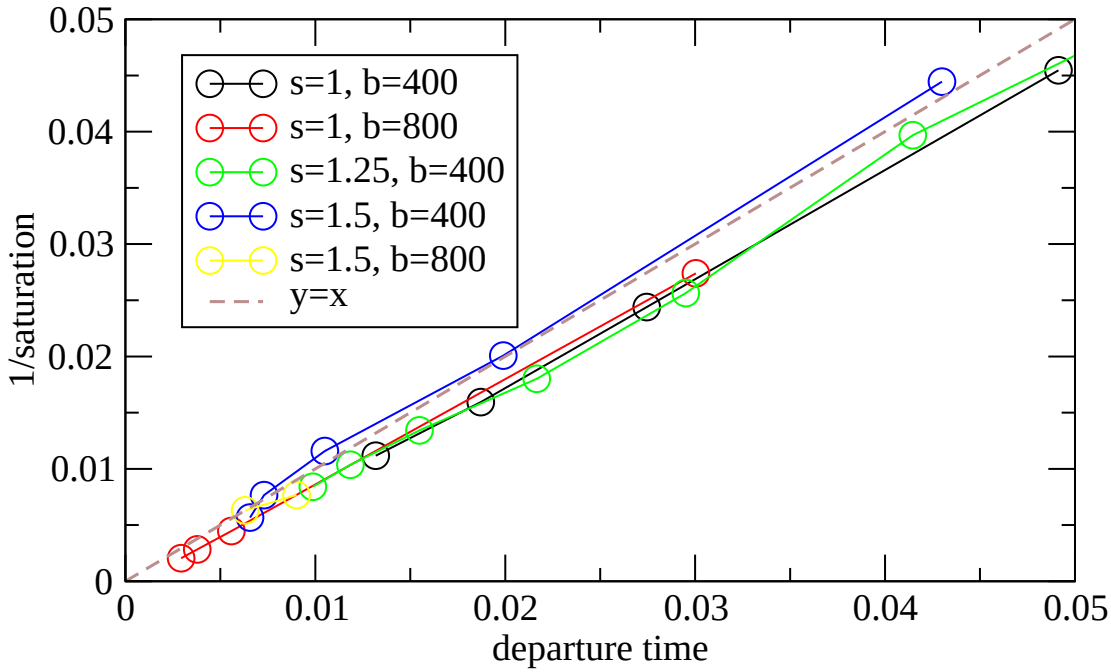

Figure 5.14: Departure time for $\delta E_{\text{core}}(t)$ in the WM versus the inverse of the saturation value. The prediction is that the departure time is the inverse of the saturation, so the theoretical line $y = x$ is drawn, and we see good agreement.

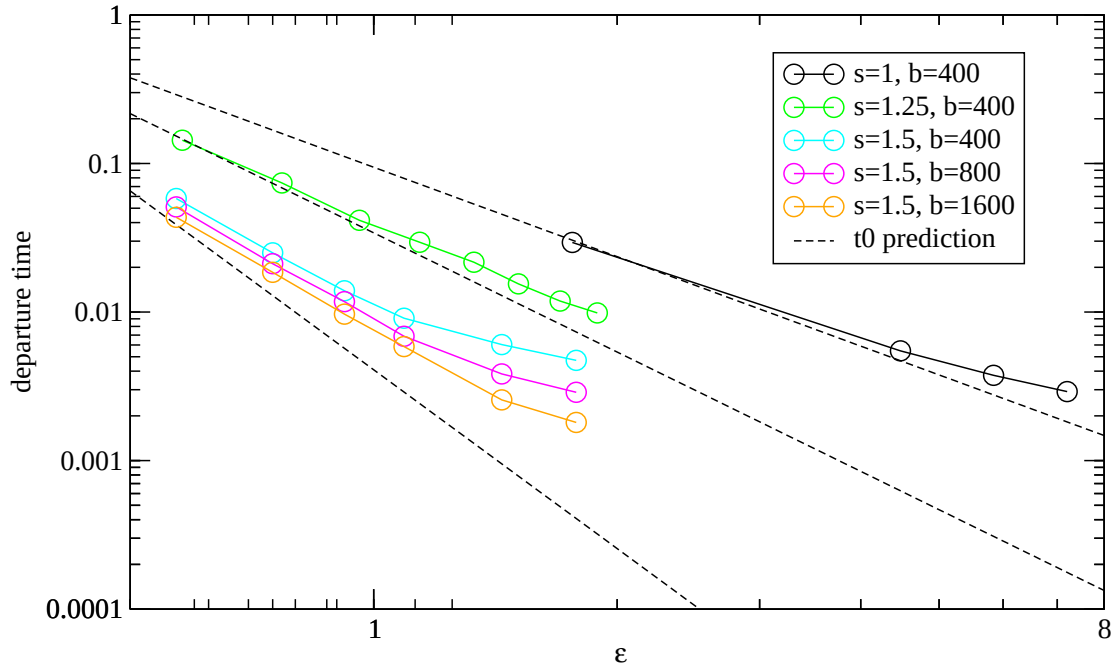

Figure 5.15: Departure time for $\delta E_{\text{core}}(t)$ with respect to perturbation strength ϵ.. The dashed line represents the expected departure time assuming the departure time goes like t_0. Observe that there is relatively good agreement for small ϵ, but systematic deviations for large ϵ. Furthermore, these deviations shrink as the bandwidth increases, demonstrating that the deviations are due to a finite size effect.

lowed us to deduce the generalized Wigner time t_0. The non-perturbative core within $\omega < \gamma_0$, however, has a non-universal structure that depends on the details of the model and in physical circumstances reflects the semi-classical dynamics in the phase space [11, 35, 16]. Indeed, we find that the LDoS of the WM and its FM counterpart have the same first order tails, while the core (for $s > 1$) is different. Consequently $P(t)$ exhibits an exponential-like decay in the WM case, but power-law decay in the FM case. It is only for the standard case of flat band-profile ($s = 1$) that both expressions coincide.

6 Concluding Remarks

Random Matrix Theory (RMT) was originally conceived half a century ago by Wigner in order to describe the statistical properties of the spectrum and eigenfunctions of complex nuclei. RMT was studied extensively due to its rich mathematical content by early pioneers such as Mehta and Porter. The physics community has also extensively drawn from RMT modeling especially in the last couple of decades due to mesoscopic systems and quantum chaos studies, i.e., the studies of quantum systems with chaotic classical dynamics. In fact, the overwhelming numerical evidence on the applicability of RMT predictions in the study of statistical properties of eigenfunctions and eigenvalues of complex chaotic systems led many people to define quantum chaos as being synonymous with systems admitting a RMT model. This is probably going too far. This dogmatic belief in RMT has been challenged and extensively investigated in recent years, by various authors leading to more careful statements on the applicability of RMT. However, these previous studies were focused on spectral and eigenfunction analysis. Following the path of Cohen and Kottos, we brought RMT modeling into the frame of quantum dynamics. Motivated by previous studies that recognized the importance of

structures in the energy landscape of quantum operators, we introduced a new ensemble of random matrices that extends the traditional Wigner theory and we investigated the resulting wave-packet dynamics scenario. Of special interest to our analysis was the investigation of the time relaxation properties of a prepared state into a sea of other states (the continuum). We found that, for a large family of RMT models with a non-flat profile, the survival probability $P(t)$ might exhibit either exponential-like or power-law decay, depending on the non-universal features of the model. This is a novel result as it takes us beyond the traditional Wigner (Fermi Golden Rule) exponential decay. We believe that our study will shed light on the design of mesoscopic dots with a controlled relaxation process, while additionally it opens the way to model the so-called "doorway states" in the energy redistribution found in atomic physics and quantum chemistry.

There is still a long way to go until we will understand completely the importance of structures in the quantum evolution of complex quantum systems. The ultimate goal is to be able to build a theory of quantum dissipation that incorporates the non-universal features (semi-classical structures) that goes beyond the standard perturbative limit. Our study constitutes a first but significant step in this direction, as it addresses wave-packet dynamics in the presence of such structures.

Appendices

A Mathematical Details

A.1 Justification of Equation (4.9) in Section 4.1.2 on p. 41

The statement we will establish is that:

$$|i\rangle = \frac{|\lambda\rangle + \sum_{\mu} c_{\mu} |\mu\rangle}{\sqrt{1 + \sum_{\mu} |c_{\mu}|^2}} \tag{4.9}$$

A priori, we can write $|i\rangle$ as a linear combination of the eigenstates of $\mathcal{H}_0$, since the set of eigenstates spans all of Hilbert space. So

$$|i\rangle = \frac{c_{\lambda} |\lambda\rangle + \sum_{\mu} c_{\mu} |\mu\rangle}{\sqrt{|c_{\lambda}|^2 + \sum_{\mu} |c_{\mu}|^2}}. \tag{A.1}$$

If $c_{\lambda} \neq 0$, then it would be possible to divide the numerator and the denominator by c_{λ} and redefine all the c_{μ}'s to include the c_{λ}. This would simplify the above expression:

It remains to be shown that $c_\lambda \neq 0$. First order time independent perturbation theory shows that the first order correction to any eigenstate $|i\rangle$ is given by

$$\sum_{k,j} \frac{V_{kj}}{E_k^{(0)} - E_j^{(0)}} |j\rangle \tag{A.2}$$

So when $|j\rangle = |\lambda\rangle$, $V_{\lambda k}$ is always nonzero. Thus there is always a nonzero contribution of $|\lambda\rangle$ to an eigenvector of $\mathcal{H}$. Therefore $c_\lambda \neq 0$, and we are free to divide by c_λ. By a harmless relabeling, we arrive at Equation (4.9).

A.2 Justification of Equation (4.14) in Section 4.1.2 on p. 44

Here we will prove Equation (4.14):

$$|\langle\lambda|i\rangle|^2 = \frac{\epsilon^2}{(\Gamma/2)^2 + (E_\lambda^{(0)} - E_i)^2}. \tag{4.14}$$

where

$$\Gamma = \frac{2\pi\epsilon^2}{\Delta}\sqrt{1 + \left(\frac{\Delta}{\pi\epsilon}\right)^2}.$$

We begin with the LDoS kernel,

$$|\langle\lambda|i\rangle|^2 = \left(1 + \sum_\mu \left[\frac{|V_{\lambda\mu}|}{E_i - E_\mu^{(0)}}\right]^2\right)^{-1} \tag{A.3}$$

We will now simplify the sum in the denominator.

$$\begin{aligned} S &= \sum_{\mu} \left[\frac{|V_{\lambda\mu}|}{E_i - E_\mu^{(0)}} \right]^2 = \epsilon^2 \sum_{k=-\infty}^{\infty} (E_i - E_\lambda^{(0)} - \Delta k)^{-2} \\ &= \frac{\epsilon^2}{\Delta^2} \sum_{k=-\infty}^{\infty} \left(\frac{E_i - E_\lambda^{(0)}}{\Delta} - k \right)^{-2} \end{aligned} \tag{A.4}$$

It is a mathematical identities that:

$$\sum_{k=-\infty}^{\infty} (z-k)^{-2} = \frac{\pi^2}{\sin^2(\pi z)}. \tag{A.5}$$

So then,

$$S = \frac{\epsilon^2}{\Delta^2} \left(\frac{\pi^2}{\sin^2\left(\pi \frac{E_i - E_\lambda^{(0)}}{\Delta} \right)} \right) = \frac{\epsilon^2 \pi^2}{\Delta^2} \sin^{-2}\left[\frac{\pi}{\Delta} (E_i - E_\lambda^{(0)}) \right]. \tag{A.6}$$

Using the Pythagorean identities that $1 + \cot^2\theta = 1/\sin^2\theta$, it is possible to write S as,

$$S = \frac{\epsilon^2 \pi^2}{\Delta^2} \left(1 + \cot^2\left[\frac{\pi}{\Delta} (E_i - E_\lambda) \right] \right). \tag{A.7}$$

We will now derive another expression using Equation (A.5) by integrating both sides of it with respect to z.

$$\begin{aligned} \int \sum_{k=-\infty}^{\infty} (z-k)^{-2}\, dz &= \int \frac{\pi^2}{\sin^2(\pi z)}\, dz \\ \therefore \cancel{(-1)} \sum_{k=-\infty}^{\infty} (z-k)^{-1} &= \frac{\cancel{-}\pi}{\tan z} = \pi \cot z \end{aligned} \tag{A.8}$$

Combining Equations (4.11b) and (4.11a) yields an expression for the following energy difference:

$$E_\lambda^{(0)} - E_i = \sum_\mu \frac{|V_{\lambda\mu}|^2}{E_\mu^{(0)} - E_i}. \tag{A.9}$$

Call this sum σ. So then,

$$\sigma = \epsilon^2 \sum_{k=-\infty}^{\infty} (E_\lambda^{(0)} + k\Delta - E_i)^{-1} = \frac{\epsilon^2}{\Delta} \sum_{k=-\infty}^{\infty} \left(\frac{E_\lambda^{(0)} - E_i}{\Delta} + k \right)^{-1}. \tag{A.10}$$

Use the identity to write that:

$$\sigma = \frac{\epsilon^2 \pi}{\Delta} \tan^{-1} \left[\frac{\pi}{\Delta} (E_\lambda^{(0)} - E_i) \right] = E_\lambda^{(0)} - E_i. \tag{A.11}$$

Now it is possible to simplify S, because we have just shown that

$$\cot^2 \left[\frac{\pi}{\Delta} (E_\lambda^{(0)} - E_i) \right] = \left(\frac{\Delta}{\epsilon^2 \pi} \right)^2 (E_\lambda^{(0)} - E_i)^2. \tag{A.12}$$

So then,

$$\begin{aligned} S &= \frac{\epsilon^2 \pi^2}{\Delta^2} \left(1 + \cot^2 \left[\frac{\pi}{\Delta} (E_i - E_\lambda^{(0)} \right] \right) = \frac{\epsilon^2 \pi^2}{\Delta^2} \left(1 + \left(\frac{\Delta}{\epsilon^2 \pi} \right)^2 (E_\lambda^{(0)} - E_i)^2 \right) \\ &= \frac{\epsilon^2 \pi^2}{\Delta^2} + \frac{1}{\epsilon^2} (E_\lambda^{(0)} - E_i)^2 \end{aligned} \tag{A.13}$$

$$|\langle\lambda|i\rangle|^2 = \frac{1}{1+S} = \frac{1}{1+\frac{\epsilon^2\pi^2}{\Delta^2}+\frac{1}{\epsilon^2}(E_\lambda^{(0)}-E_i)^2} = \frac{\epsilon^2}{\epsilon^2+\frac{\epsilon^4\pi^2}{\Delta^2}+(E_\lambda^{(0)}-E_i)^2} \quad \text{(A.14)}$$

Define the quantity Γ in the following way:

$$\epsilon^2 + \frac{\epsilon^4\pi^2}{\Delta^2} = \frac{\epsilon^4\pi^2}{\Delta^2}\left(\frac{\Delta^2}{\pi^2\epsilon^2}+1\right) = \left(\frac{\Gamma}{2}\right)^2$$
$$\therefore \Gamma = \frac{2\pi\epsilon^2}{\Delta}\sqrt{1+\left(\frac{\Delta}{\pi\epsilon}\right)^2}.$$

B LDoS, Green's Functions, and Spectral Functions

B.1 The LDoS and its Relationship with the Green's Function

It is an identity that:

$$G^{\pm}(\omega) = \frac{1}{\omega \pm 0i - \mathcal{H}} = \frac{1}{\omega - \mathcal{H}} \mp i\pi\delta(\omega - \mathcal{H}) \tag{B.1}$$

where "0" denotes an infinitesimal. This can be shown using contour integration in the complex plane. From the above statement, observe that,

$$\mathrm{Im}\left[G^{+}\right] = \frac{i}{2}[G^{+} - G^{-}] = -\pi\delta(E - \mathcal{H}). \tag{B.2}$$

Now it will be shown that sandwiching $-\frac{1}{\pi}\mathrm{Im}\left[G^{+}\right]$ with $|\Psi\rangle$ yields the local density of states (LDoS), $\rho(\omega)$.

$$\begin{aligned}\langle\Psi|\,\frac{-1}{\pi}\mathrm{Im}\left[G^{+}\right]|\Psi\rangle &= \langle\Psi|\,\delta(E-\mathcal{H})\,|\Psi\rangle \\ &= \langle\Psi|\,\delta(E-\mathcal{H})\left(\sum_{n}|n\rangle\langle n|\right)|\Psi\rangle \\ &= \sum_{n}|\langle\Psi|n\rangle|^{2}\delta(E-E_{n}) \qquad \text{(B.3)}\end{aligned}$$

which is exactly the definition of the LDoS. So,

$$\rho(E) = -\frac{1}{\pi}\langle\Psi|\,\mathrm{Im}\left[G^{+}\right]|\Psi\rangle\,. \qquad \text{(B.4)}$$

B.2 Feshbach's Projection Method and Retarded Green's Functions

The derivation here is based on the setup discussed in Section 5.1 This method of partition the Hamiltonian is due to Feshbach [36]. Without loss of generality, write the Hamiltonian $\mathcal{H}$ in the basis of $\mathcal{H}_0$ in the following form:

$$\mathcal{H} = \begin{pmatrix} E_\lambda & \sigma_1 & \sigma_2 & \sigma_3 & \cdots & \sigma_k & \cdots \\ \sigma_1 & E_1 & 0 & 0 & \cdots & 0 & \cdots \\ \sigma_2 & 0 & E_2 & 0 & \cdots & 0 & \cdots \\ \sigma_3 & 0 & 0 & E_3 & & \vdots & \\ \vdots & \vdots & \vdots & & \ddots & 0 & \\ \sigma_k & 0 & 0 & \cdots & 0 & E_k & \\ \vdots & \vdots & \vdots & & & & \ddots \end{pmatrix}$$

Note that the bound state $|\lambda\rangle$ corresponds to the energy E_λ in the first row and column, but this is only for aesthetic considerations. The argument described below does not assume this is the lowest energy level.

Since we only care about the state $|\lambda\rangle$, we decompose the system into two subspaces. One that is simply the state $|\lambda\rangle$, and the other subspace is all of Hilbert space excluding the space containing $|\lambda\rangle$.

$$\mathcal{H} = \begin{pmatrix} \mathcal{H}_0^P & 0 \\ 0 & \mathcal{H}_0^Q \end{pmatrix} + \begin{pmatrix} 0 & V^{PQ} \\ V^{QP} & 0 \end{pmatrix} \tag{B.5}$$

So apparently $\mathcal{H}_0^P$ is a 1×1 matrix, $\mathcal{H}_0^Q$ is an $\infty\times\infty$ matrix, V^{PQ} is a $1\times\infty$ vector, and V^{QP} is an $\infty \times 1$ vector. Consider an eigenstate of $\mathcal{H}$ called $\Psi = (\psi \quad \chi)^{\mathrm{T}}$. Then,

$$\begin{pmatrix} \mathcal{H}_0^P & V^{PQ} \\ V^{QP} & \mathcal{H}_0^Q \end{pmatrix} \begin{pmatrix} \psi \\ \chi \end{pmatrix} = E \begin{pmatrix} \psi \\ \chi \end{pmatrix} \tag{B.6}$$

From the second row of the above equation, we can see that $\chi = G_0^Q V^{QP}\psi$ where $G_0^Q = (E\mathbb{1} - \mathcal{H}_0^Q)^{-1}$. Taking the first row of the equation, and substituting for χ, we find that,

$$[\mathcal{H}_0^P + V^{PQ}G_0^Q V^{QP}]\psi = E\psi. \tag{B.7}$$

The next step is to lift E to the complex plane and rewrite G_0^Q as,

$$G_0^Q = \frac{1}{(E+0i)\mathbb{1} - \mathcal{H}_0^Q} = \frac{1}{E\mathbb{1} - \mathcal{H}_0^Q} - i\pi\delta(E\mathbb{1}). \tag{B.8}$$

Where we have used the Cauchy Principle Value. We then can proceed to rewrite part of the left hand side of Equation (B.7),

$$\begin{aligned} V^{PQ}G_0^Q V^{QP} &= V^{PQ}\left(\frac{1}{E\mathbb{1} - \mathcal{H}_0^Q} - i\pi\delta(E\mathbb{1})\right)V^{QP} \\ &= V^{PQ}\frac{1}{E\mathbb{1} - \mathcal{H}_0^Q}V^{QP} - i\pi V^{PQ}\delta(E\mathbb{1})V^{QP} \\ &= \sum_n \frac{|V_{\lambda,n}|^2}{E - E_n} - i\pi\sum_m |V_{\lambda,m}|^2\delta(E - E_m). \end{aligned} \tag{B.9}$$

Substituting the above into Equation (B.7) provides us with the effective Hamiltonian for the state $|\lambda\rangle$, $\mathcal{H}_P$,

$$\mathcal{H}^P = \mathcal{H}_0^P + V^{PQ}G_0^Q V^{QP} = \mathcal{H}_0^P + \Delta(E) - i\Gamma(E)/2 \tag{B.10}$$

where

$$\Delta(E) = \sum_n \frac{|V_{\lambda,n}|^2}{E - E_n}$$
$$\Gamma(E) = 2\pi \sum_m |V_{\lambda,m}|^2 \delta(E - E_m) \tag{B.11}$$

Note that $\mathcal{H}^P$ is non-Hermitian because probability can leak into the space Q. For the LDoS analysis, we are interested in the quantity $\langle\lambda| G^+ |\lambda\rangle$ where G^+ is the retarded Green's function of the full Hamiltonian $\mathcal{H}$. But the dynamics of $|\lambda\rangle$ is determined by $\mathcal{H}^P$, so we argue that $\langle\lambda| G^+ |\lambda\rangle$ is the same as $\langle\lambda| G^P |\lambda\rangle$ where G^P is the retarded Green's function for the effective Hamiltonian, $\mathcal{H}^P$. Furthermore, G^P is a 1×1 matrix because $\mathcal{H}^P$ is a 1×1 matrix, so we have that $\langle\lambda| G^P |\lambda\rangle = G^P$. And thus,

$$\begin{aligned} \langle\lambda| G^+ |\lambda\rangle &= \langle\lambda| G^P |\lambda\rangle = G^P(\omega) \\ &= \frac{1}{\omega - \mathcal{H}^P} = \frac{1}{\omega - E_\lambda - \Delta(\omega) + i\Gamma(\omega)/2} \end{aligned} \tag{B.12}$$

Replacing $\omega - E_\lambda \mapsto \omega$ yields the general expression

$$\langle\lambda| G^+ |\lambda\rangle = \frac{1}{(\omega - \Delta(\omega)) + i\Gamma(\omega)/2} \tag{B.13}$$

The argument in Appendix B.1 shows that the imaginary part of this is the LDoS. To find the imaginary part, we will clear the denominator of its imaginary part. The functions $\Gamma(\omega)$ and $\Delta(\omega)$ are real valued, so it is simple to multiply the

numerator and denominator by the complex conjugate of the denominator.

$$\begin{aligned}\langle\lambda|\, G^{+}\,|\lambda\rangle &= \frac{1}{(\omega-\Delta(\omega))+i(\Gamma(\omega)/2)}\frac{(\omega-\Delta(\omega))-i(\Gamma(\omega)/2)}{(\omega-\Delta(\omega))-i(\Gamma(\omega)/2)} \\ &= \frac{\omega-\Delta(\omega)}{(\omega-\Delta(\omega))^2+(\Gamma(\omega)/2)^2}+i\frac{-\Gamma(\omega)/2}{(\omega-\Delta(\omega))^2+(\Gamma(\omega)/2)^2}\end{aligned}$$

So by inspection,

$$-\langle\lambda|\,\mathrm{Im}\left[G^{+}\right]|\lambda\rangle = \frac{-\Gamma(\omega)/2}{(\omega-\Delta(\omega))^2+(\Gamma(\omega)/2)^2}. \tag{B.14}$$

Therefore, we have shown that:

$$\rho(\omega) = \frac{1}{\pi}\frac{\Gamma(\omega)/2}{(\omega-\Delta(\omega))^2+(\Gamma(\omega)/2)^2}. \tag{B.15}$$

B.3 Evaluation of Spectral Functions

The Green's function analysis reveals two spectral functions, $\Gamma(\omega)$ and $\Delta(\omega)$. In order to have a complete expression for the LDoS, it is necessary to evaluate these functions.

$$\Delta(\omega) = \sum_{n\neq\lambda}\frac{|V_{n,\lambda}|^2}{E_\lambda - E_n} = \int_{-\infty}^{\infty}\frac{\tilde{C}(\omega')}{\omega-\omega'}d\omega'. \tag{B.16}$$

Thus,

$$\Delta(\omega) = \int_{-\infty}^{\infty}\frac{\epsilon^2|\omega'|^{s-1}}{\omega-\omega'}d\omega' \tag{B.17}$$

This can be evaluated in a Computer Algebra System (such as Mathematica), and it simplifies to:

$$\Delta(\omega) = \epsilon^2 \pi \omega |\omega|^{s-2} \cot \frac{s\pi}{2} \tag{B.18}$$

The $\Gamma(\omega)$ term easily evaluated, it is simply:

$$\Gamma(\omega) = 2\pi \sum_n |V_{\lambda,n}|^2 \delta(\omega - E_n) \equiv 2\pi \tilde{C}(\omega) = 2\pi\epsilon^2 |\omega|^{s-1}. \tag{B.19}$$

C Scaling Relations for $\delta E_{\text{tails}}(t)$

We will now describe the δE_{tails} scaling for systems with power spectrum $\tilde{C}(\omega) = \epsilon^2|\omega|^{s-1}$ and cutoff ω_c. Thus, the flat band-profile situation is the special case $s = 1$. It is a result in Linear Response Theory (see [16]) that,

$$\delta E_{\text{tails}}(t) = \sqrt{2[C(0) - C(t)]}. \tag{C.1}$$

where $C(t)$ is the autocorrelation function. As t approaches infinity, $C(t)$ tends towards zero. So the asymptotic value of $\delta E_{\text{tails}}(t)$ is $\sqrt{2C(0)}$. It is possible to compute $C(0)$ because its Fourier transform, $\tilde{C}(\omega)$, is known.

$$C(0) = \frac{1}{2\pi}\int_{-\infty}^{\infty} \tilde{C}(\omega)e^{-(0)\omega}d\omega = \frac{1}{\pi}\epsilon^2\int_0^{\omega_c} \omega^{s-1}d\omega = \frac{\epsilon^2\omega_c^s}{s\pi} \tag{C.2}$$

So apparently the scaling of δE_{tails} is $\delta E_{\text{tails}} \mapsto \sqrt{\frac{s}{\epsilon^2\omega_c^s}}\delta E_{\text{tails}}$. In order to understand the time scale of $\delta E_{\text{tails}}(t)$, expand $C(t)$ about zero.

$$C(t) = \sum_{n=0}^{\infty} \frac{C^{(n)}(0)}{n!}t^n \tag{C.3}$$

It is necessary to compute the n^{th} derivatives of $C(t)$ evaluated at zero. Fortunately, this can be done.

$$\begin{aligned}
\frac{d^n C(t)}{dt^n}\Big|_{t=0} &= \frac{1}{2\pi}\int_{-\infty}^{\infty}\tilde{C}(\omega)\frac{d^n e^{i\omega t}}{dt^n}d\omega\Big|_{t=0} \\
&= \frac{1}{2\pi}\int_{-\infty}^{\infty}\epsilon^2|\omega|^{s-1}(i\omega)^n e^{i\omega t}d\omega\Big|_{t=0} \\
&= \frac{i^n\epsilon^2}{2\pi}\int_{-\omega_c}^{\omega_c}|\omega|^{s-1}\omega^n d\omega
\end{aligned} \tag{C.4}$$

When n is odd, the integrand is odd, and because the interval is symmetric, the integral evaluates to zero. For n even,

$$\begin{aligned}
\frac{d^n C(t)}{dt^n}\Big|_{t=0} &= \frac{i^n\epsilon^2}{\pi}i^n\epsilon^2\int_0^{\omega_c}\omega^{s+n-1}d\omega \\
&= \frac{i^n\epsilon^2}{\pi}\frac{\omega_c^{s+n}}{s+n}
\end{aligned} \tag{C.5}$$

So then the expansion of $C(t)$ to second order is,

$$C(t) = C(0) - \frac{\omega_c^{s+2}\epsilon^2}{2\pi(s+2)}t^2 + \cdots \tag{C.6}$$

So we have that,

$$\begin{aligned}
\delta E_{\text{tails}}(t) &\approx \sqrt{\frac{\omega_c^{s+2}\epsilon^2}{(s+2)\pi}t^2} \\
\sqrt{\frac{s}{\epsilon^2\omega_c^s}}\delta E_{\text{tails}}(t) &\approx \sqrt{\frac{s}{\epsilon^2\omega_c^s}}\sqrt{\frac{2\omega_c^{s+2}\epsilon^2}{(s+2)\pi}t^2} \\
\sqrt{\frac{s}{\epsilon^2\omega_c^s}}\delta E_{\text{tails}}(t) &\approx \frac{1}{\sqrt{\pi}}\sqrt{\frac{s}{(s+2)}}\omega_c t
\end{aligned} \tag{C.7}$$

So then apparently the time scaling is $t \mapsto \sqrt{\frac{s}{s+2}}\omega_c t$.

Bibliography

[1] E. P. Wigner. Characteristic vectors of bordered matrices with infinite dimensions. *The Annals of Mathematics*, 62(3):548–564, 1955.

[2] M. L. Mehta. *Random matrices and the statistical theory of energy levels*. Academic Press, 1967.

[3] H. J. Stöckmann. *Quantum chaos: an introduction*. Cambridge University Press, 1999.

[4] Y. Alhassid. The statistical theory of quantum dots. *Rev. Mod. Phys.*, 72(4):895–968, Oct 2000.

[5] F. Haake. *Quantum Signatures of Chaos*. Springer-Verlag New York, Inc., Secaucus, NJ, USA, 2006.

[6] T. Kottos and U. Smilansky. Periodic orbit theory and spectral statistics for quantum graphs. *Annals of Physics*, 274(1):76–124, 1999.

[7] H. Schanz and T. Kottos. Scars on quantum networks ignore the lyapunov exponent. *Phys. Rev. Lett.*, 90(23):234101, Jun 2003.

[8] L. Kaplan and E. J. Heller. Measuring scars of periodic orbits. *Phys. Rev. E*, 59(6):6609–6628, Jun 1999.

[9] D. Cohen, F. M. Izrailev, and T. Kottos. Wave packet dynamics in energy space, random matrix theory, and the quantum-classical correspondence. *Phys. Rev. Lett.*, 84(10):2052–2055, Mar 2000.

[10] D. Cohen and T. Kottos. Quantum-mechanical nonperturbative response of driven chaotic mesoscopic systems. *Phys. Rev. Lett.*, 85(23):4839–4843, Dec 2000.

[11] T. Kottos and D. Cohen. Failure of random matrix theory to correctly describe quantum dynamics. *Phys. Rev. E*, 64(6):065202, Nov 2001.

[12] T. Kottos and D. Cohen. Quantum irreversibility of energy spreading. *EPL (Europhysics Letters)*, 61(4):431–437, 2003.

[13] D. Cohen and T. Kottos. Non-perturbative response: chaos versus disorder. *Journal of Physics A: Mathematical and General*, 36(40):10151–10158, 2003.

[14] D. Cohen and T. Kottos. Quantum dissipation due to the interaction with chaos. *Physical Review E (Statistical, Nonlinear, and Soft Matter Physics)*, 69(5):055201, 2004.

[15] M. Hiller, T. Kottos, D. Cohen, and T. Geisel. Quantum reversibility: Is there an echo? *Physical Review Letters*, 92(1):010402, 2004.

[16] M. Hiller, D. Cohen, T. Geisel, and T. Kottos. Wavepacket dynamics, quantum reversibility and random matrix theory. *Annals of Physics*, 321:1025, 2006.

[17] J. Aisenberg, I. Sela, T. Kottos, D. Cohen, and A. Elgart. Anomalous decay of a prepared state due to non-ohmic coupling to the continuum. Manuscript in preparation, 2009.

[18] J. Bodyfelt. Probing complex dynamics via loschmidt echoes. 2009.

[19] M. V. Berry. *Chaos and quantum physics*. North-Holland, 1991.

[20] Y. Imry. *Introduction to mesoscopic physics*. Oxford University Press, USA, 2002.

[21] M. Feingold and A. Peres. Distribution of matrix elements of chaotic systems. *Phys. Rev. A*, 34(1):591–595, Jul 1986.

[22] T. Prosen and M. Robnik. Distribution and fluctuation properties of transition probabilities in a system between integrability and chaos. *Journal of Physics A: Mathematical and General*, 26(6):–319, 1993.

[23] D. Cohen and T. Kottos. Parametric dependent hamiltonians, wavefunctions, random-matrix-theory, and quantal-classical correspondence. *Physical Review E*, 63:36203, 2001.

[24] C. C. Abilio, P. Butaud, T. Fournier, B. Pannetier, J. Vidal, S. Tedesco, and B. Dalzotto. Magnetic field induced localization in a two-dimensional superconducting wire network. *Phys. Rev. Lett.*, 83(24):5102–5105, Dec 1999.

[25] D. Cohen, T. Kottos, and H. Schanz. Rate of energy absorption by a closed ballistic ring. *Journal of Physics A: Mathematical and General*, 39(38):11755–11771, 2006.

[26] M. Hiller, T. Kottos, and T. Geisel. Complexity in parametric bose-hubbard hamiltonians and structural analysis of eigenstates. *Physical Review A (Atomic, Molecular, and Optical Physics)*, 73(6):061604, 2006.

[27] O. Bohigas. *Chaos and quantum physics*. North-Holland, 1991.

[28] M. V. Berry and M. Tabor. Level clustering in the regular spectrum. *Proceedings of the Royal Society of London. A. Mathematical and Physical Sciences*, 356(1686):375–394, 1977.

[29] M. V. Berry. Regular and irregular semiclassical wavefunctions. *Journal of Physics A: Mathematical and General*, 10(12):2083–2091, 1977.

[30] C. Cohen-Tannoudji, J. Dupont-Roc, and G. Grynberg. *Atom-photon interactions*. Wiley New York, 1998.

[31] J. L. Gruver, J. Aliaga, H. A. Cerdeira, P. A. Mello, and A. N. Proto. Energy-level statistics and time relaxation in quantum systems. *Phys. Rev. E*, 55(6):6370–6376, Jun 1997.

[32] F. J. Dyson and M. L. Mehta. Statistical theory of the energy levels of complex systems. iv. *Journal of Mathematical Physics*, 4(5):701–712, 1963.

[33] A. Barnett, D. Cohen, and E. J. Heller. Deformations and dilations of chaotic

billiards: Dissipation rate, and quasiorthogonality of the boundary wave functions. *Phys. Rev. Lett.*, 85(7):1412–1415, Aug 2000.

[34] M. Feingold. Density of states for banded and sparse random matrices. *EPL (Europhysics Letters)*, 17(2):97–102, 1992.

[35] J. A. Mendez-Bermudez, T. Kottos, and D. Cohen. The twilight zone in the parametric evolution of eigenstates: beyond perturbation theory and semiclassics. *Physical Review E*, 72:027201, 2005.

[36] A. de Shalit and H. Feshbach. *Theoretical nuclear physics, Vol. 1.* Wiley, New York, 1974.